Mechanical overstimulation causes acute injury followed by fast recovery in lateral-line neuromasts of larval zebrafish

Melanie Holmgren[1], Michael E. Ravicz[2,3], Kenneth E. Hancock[2,3], Olga Strelkova[2,3], Artur A. Indzhykulian[2,3], Mark E. Warchol[1], Lavinia Sheets[1]*

1. Department of Otolaryngology, Washington University School of Medicine, St. Louis, MO, USA
2. Eaton-Peabody Laboratory, Massachusetts Eye and Ear, Boston, Massachusetts, USA
3. Department of Otolaryngology–Head and Neck Surgery, Harvard Medical School, Boston, Massachusetts, USA

*** Corresponding author**
Lavinia Sheets: sheetsl@wustl.edu

Abstract

Noise exposure damages sensory hair cells, resulting in loss of synaptic connections with auditory nerves and hair-cell death. The cellular mechanisms underlying noise-induced hair-cell damage and subsequent repair are not completely understood. Hair cells in neuromasts (NMs) of larval zebrafish are structurally and functionally comparable to mammalian hair cells but undergo robust regeneration following damage. We therefore developed a model for noise-induced hair-cell damage in this highly tractable system. Free swimming larvae exposed to strong water current for 2 hours displayed damage to NMs, including synapse loss, afferent neurite retraction, damaged hair bundles, and reduced mechanotransduction. Overstimulation also elicited an inflammatory response and macrophage recruitment. Remarkably, NM morphology and function appeared to fully recover within 2 days following exposure. Our results reveal morphological and functional changes in mechanically overstimulated lateral-line NMs that are analogous to changes observed in noise-exposed mammalian ear yet are rapidly and completely repaired.

Keywords: Hair cell, noise damage, ribbon synapse, inflammation, regeneration

Introduction

Hair cells are the sensory receptors of the inner ear and lateral-line organs that detect sound, orientation, and motion. They transduce these stimuli though deflection of stereocilia, which opens mechanically-gated cation channels (LeMasurier & Gillespie, 2005; Qiu & Muller, 2018) and drives subsequent transmission of sensory information via excitatory glutamatergic synapses (Glowatzki & Fuchs, 2002). Excessive stimulation, such as loud noise, can damage hair cells and their synaptic connections to afferent nerves. The degree of damage depends on the intensity and duration of the stimulus, with higher levels of traumatic noise leading to hair-cell loss (Cho et al., 2013; Nordmann, Bohne, & Harding, 2000) and lower levels leading to various pathologies, including damage to the hair-cell mechanotransduction complex/machinery and stereocilia (Gao, Ding, Zheng, Ruan, & Liu, 1992; Husbands, Steinberg, Kurian, & Saunders, 1999), misshapen hair cells (Bullen, Anderson, Bakay, & Forge, 2019), synaptic terminal damage, neurite retraction, and hair-cell synapse loss (Fernandez et al., 2020; Henry & Mulroy, 1995; Kujawa & Liberman, 2009; Puel, Ruel, Gervais d'Aldin, & Pujol, 1998). In addition to directly damaging hair cells, excess noise also initiates an inflammatory response (Hirose, Discolo, Keasler, & Ransohoff, 2005; Kaur et al., 2019; Kaur et al., 2015). Such inflammation is mediated by macrophages, a class of leukocyte that responds to injury by clearing cellular debris and promoting tissue repair (Wynn & Vannella, 2016).

The variety of injury and range of severity suggests multiple signaling pathways are involved in noise-induced hair-cell damage. Also unknown are the cellular processes mediating repair following noise damage. While hair cells show a partial capacity for repair of stereocilia and synaptic connections, some sub-lethal damage to hair cells is permanent. Numerous studies of the mammalian cochlea suggest that a subgroup of inner hair-cell synapses are permanently lost following noise exposure (Cho et al., 2013; Hickman, Smalt, Bobrow, Quatieri, & Liberman, 2018; Shi et al., 2013). Glutamate excitotoxicity is likely the pathological event that initiates noise-induced hair-cell synapse loss (Hu, Rutherford, & Green, 2020; Kim et al., 2019; Puel et al., 1998), but the downstream cellular mechanisms are still undefined.

Zebrafish have proven to be a valuable model system for studying the molecular basis of hair cell injury and repair. Zebrafish sensory hair cells are structurally and functionally homologous to mammalian hair cells (Coffin, Kelley, Manley, & Popper, 2004; Kindt & Sheets, 2018; Sebe et al., 2017). In contrast to other vertebrate model organisms, zebrafish hair cells are optically accessible in whole larvae within the lateral-line organs. These sensory organs, called neuromasts (NMs), contain clusters of ~ 14 hair cells each and are distributed throughout the external surface of the fish to detect local water movements. Zebrafish are able to

regenerate complex tissues, including lateral-line organs (Kniss, Jiang, & Piotrowski, 2016; Xiao et al., 2015). This capacity for regeneration combined with optical accessibility allows us to study cellular and synaptic damage and repair *in vivo* following mechanical trauma.

In order to model 'noise' damage in zebrafish lateral-line organs, we developed a protocol to mechanically overstimulate the lateral line of free-swimming larvae. Using this protocol, we were able to induce morphological damage to lateral-line organs analogous to what is observed in mammalian ears exposed to acoustic trauma. We observed loss of some synapses and enlargement of postsynaptic densities (PSDs) in all exposed NMs as well as hair-cell loss and afferent neurite retraction in a subset of NMs. Hair cell mechanotransduction, as measured by uptake of the cationic dye FM1-43, was significantly reduced after mechanical overstimulation. We also observed an inflammatory response similar to that observed in the mammalian cochlea after noise trauma. Remarkably, lateral-line damage appeared to rapidly recover; hair-cell number and morphology returned to normal within 4 - 8 hours following overstimulation, concurrent with clearance of cellular debris by macrophages. Additionally, NMs showed partial recovery of afferent innervation, FM1-43 uptake, and hair-cell synapse number within 2 hours following exposure, and completely recovered by 2 days post-exposure, indicating that noise-exposed NM hair cells fully repair following mechanical damage.

Results

Overstimulation of zebrafish lateral-line hair cells

To directly overstimulate hair cells of lateral-line organs in free-swimming 7-day-old zebrafish, we developed a mechanical stimulation protocol using an electrodynamic shaker to create a strong water current (Fig.1 A). Dorsal-ventral displacement of a 6-well dish at 60 Hz and acceleration of 43 m/s^2 (153 dB re 1$\mu m/s^2$) created water flow and disturbance of the water surface that was strong enough to trigger 'fast start' escape responses—a behavior mediated in part by zebrafish larval lateral-line organs to escape predation (Fig 1 B inset) (McHenry, Feitl, Strother, & Van Trump, 2009; Nair, Azatian, & McHenry, 2015). 'Fast start' escape responses can be activated by stimulating hair cells of the lateral line and/or the posterior macula in the ear (Bhandiwad, Zeddies, Raible, Rubel, & Sisneros, 2013). To verify that the observed escape responses were mediated predominantly by flow sensed by lateral-line hair cells rather than hair cells of the macula, we exposed a group of larvae to 3μM of copper sulfate ($CuSO_4$) prior to noise to specifically ablate lateral-line hair cells, but leave hair cells of the ear intact (Olivari, Hernandez, & Allende, 2008). We then recorded their behavior with a high-speed camera during stimulus (1000 fps for 10 s) and compared fish with lesioned lateral-line organs with that of untreated control siblings (Fig 1 B,C; Movie S1,2). When we ablated larval lateral-line

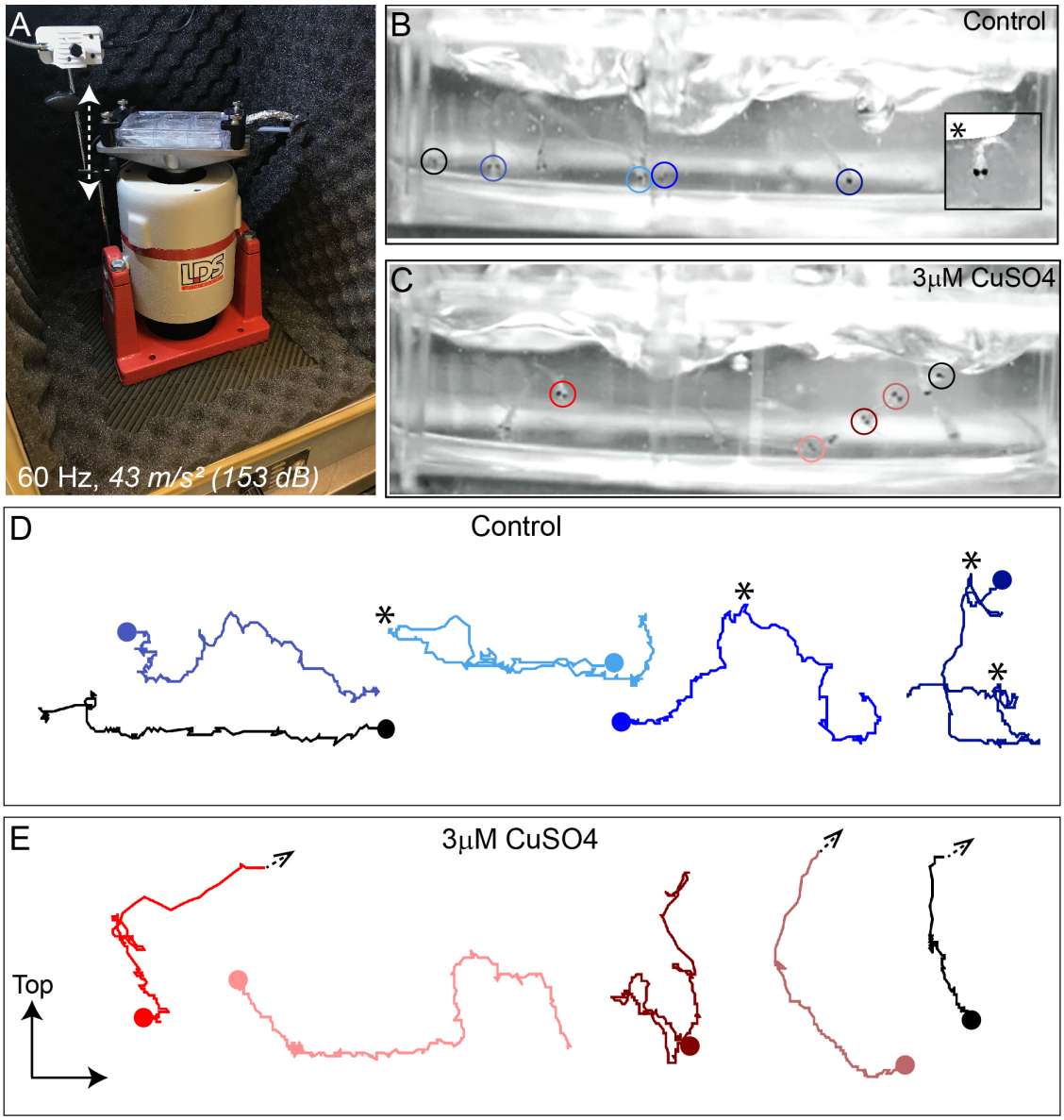

Figure 1: Intense current produced by shaker apparatus stimulates lateral-line hair cells and evokes a relevant behavior response. **(A)** The apparatus: a magnesium head expander holding a 6-well dish mounted on a vertically oriented electrodynamic shaker housed inside a sound-attenuation chamber. The stimulus consisted of a 60 Hz vertical displacement of the plate (hatched arrows) driven by an amplifier and controlled by a modified version of the Eaton-Peabody Laboratory Cochlear Function Test Suite. **(B,D)** Swimming behavior of 7-day-old larvae during noise exposure. Traces in (D) represent tracking of corresponding circled fish over 500 ms (1000 fps/ 500 frames). Asterisks indicate a "fast escape" response (B; inset). **(C,E)** Swimming behavior of larvae whose lateral-line NMs were ablated with $CuSO_4$. Arrows in (E) indicate where a larva was swept into the waves and could no longer tracked.

hair cells with $CuSO_4$ and tracked swimming behavior during noise exposure, we found that 'fast start' responses—defined as a c-bend of the body occurring within 15 ms followed by a counter-bend (Burgess & Granato, 2007; McHenry et al., 2009)—occurred far less frequently than in

siblings with intact lateral line (Fig 1 C,E; avg. 'fast start' responses: : 0.4 (± 0.1)/s in lateral-line ablated vs 1.5 (± 0.1)/s in control; 3 trials,10 s per trial). Accordingly, some $CuSO_4$-treated fish were unable to escape the current and were swept into the waves (Fig 1 E; arrowheads; Movie S2). These observations indicate that the strong current generated by our device is stimulating lateral-line hair cells and evoking a behaviorally relevant response.

Morphological damage to NMs depends on the time distribution of mechanical overstimulation and position of NM

To compare mechanical stress from overstimulation exposures with different time distributions, zebrafish (10-15 per well) were exposed to an initial 20 minutes of stimulus followed by 10 minutes of rest, then either 2 hours of continuous (sustained) or intermittent (periodic) noise (Fig 2 B). The ten-minute break in the sustained exposure was introduced early on when establishing the noise-exposure protocol because it appeared to enhance larval survival; it was therefore maintained throughout the study for consistency. Fish were euthanized and fixed immediately after exposure, then processed for immunohistofluorescent labeling of hair cells and neurons. Unexposed sibling fish served as controls. As posterior lateral-line (pLL) NMs have been shown to specifically initiate escape behavior in response to strong stimuli (Liao & Haehnel, 2012), blind analysis of the morphology of pLL NMs L3, L4, and L5 was conducted for exposed and control larvae (Fig 2 A). Initially, we divided observed NM hair-cell morphology into two categories: "normal", in which hair cells were radially organized with a relatively uniform shape and size, and "disrupted", in which the hair cells were misshapen and displaced to one side, with the apical ends of the hair cells localized anteriorly (Fig 2 C,C'). Immediately following sustained exposure, 46% of exposed NMs showed a "disrupted" phenotype, whereas following a periodic exposure only 17% of the NMs appeared "disrupted" (Fig 2 D; Unpaired t-test **P=0.0034). When exposed to 140 minutes of completely uninterrupted stimulus, we observed the majority of NMs (10/12 compared with 0/13 in unexposed controls) appeared disrupted. Therefore, the degree of NM morphological disruption appears to correspond to the distribution of noise exposure i.e. intermittent exposure caused less NM disruption than continuous exposure. Position of the NM along the tail was also associated with vulnerability to disruption; we observed a gradient of damage in the pLL from rostral to caudal i.e. L5 was more susceptible to disruption than L4, which was more susceptible to disruption than L3 (Fig 2 E; Repeated measure One-way ANOVA **P=0.0016 sustained, *P=0.0400 periodic).

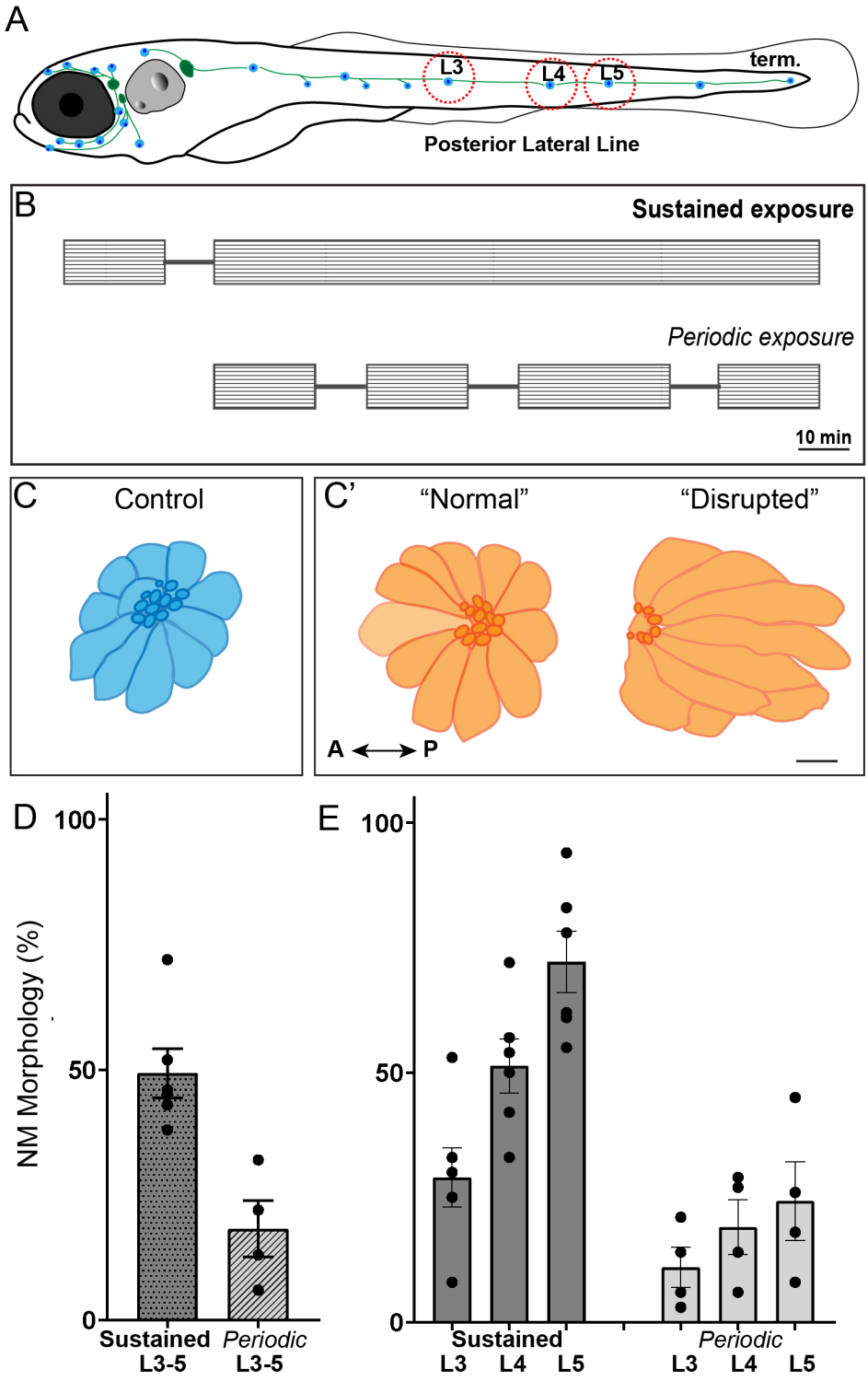

Figure 2: Morphological changes in pLL NM hair cells exposed to sustained or periodic noise stimuli. **(A)** Schematic of a larval zebrafish. Blue dots indicate hair cells of the lateral-line organs; green lines indicate innervating afferent lateral-line nerves. pLL NMs L3, L4, and L5 were analyzed (dashed circles). **(B)** Schematic of the two exposure protocols. Sustained exposure was a 20 min. pulse followed by 120 minutes uninterrupted noise; periodic exposure was 90 min. noise with intermittent 10 min. breaks totaling 120 minutes. **(C-C')** Schematic of dorsal top-down 2D projections of control (C) or noise-exposed (C') NM hair cells. Exposed NM hair-cell morphology was categorized as "normal" i.e. radial hair-cell organization indistinguishable from control or "disrupted" i.e. asymmetric organization with the hair-cell apical ends oriented anteriorly (Scale bar: 5μm; arrow indicates the anterior/ posterior axis). **(D-E)** Average percentage of exposed NMs with "disrupted" morphology following noise exposure. Each dot represents the percentage of disrupted NMs in a single experimental trial. Disrupted hair-cell morphology was exposure time and place dependent, with NMs more frequently disrupted following sustained stimulus and when localized toward the posterior end of the tail (E).

Impaired mitochondrial function influences hair-cell vulnerability to noise and ototoxic drugs (Alassaf, Daykin, Mathiaparanam, & Wolman, 2019; Bottger & Schacht, 2013). To determine if NM hair cells with impaired mitochondrial function were more vulnerable to noise-induced disruption, we examined zebrafish with a mutation in *mpv17* (D'Agati et al., 2017; Krauss et al., 2013). In *mpv17* (-/-) NM hair cells, we observed significantly elevated levels of cytosolic reactive oxygen species (ROS) relative to their wild-type siblings (Supplemental Fig. 1 A-C), indicating impaired mitochondrial function and corresponding with previous reported observations from embryonic fibroblasts from *Mpv17*$^{-/-}$ mice where ROS was elevated (Antonenkov et al., 2015). When exposed to sustained stimulation, *mpv17* (-/-) NMs were more vulnerable to disruption than wild-type siblings simultaneously exposed to the same stimulus (67±12% disrupted in *mpv17* (-/-) vs. 49±9% disrupted in WT siblings, Trial N=4). In mutants, we observed a gradient of NM disruption from L3 to L5 similar to what was observed in WT siblings (Supplemental Fig. 1 D). Cumulatively, these observations support that disruption of hair-cell morphology observed in a subset of NMs corresponds with more severe damage from overstimulation.

Hair-cell loss and loss of afferent nerve contacts correspond to NM disruption while hair-cell synapse loss occurs in both "normal" and "disrupted" mechanically overstimulated NMs

Moderate overstimulation of the cochlea can cause damage to or loss of hair-cell synapses, including swelling and retraction of afferent nerve fibers, while more severe exposure leads to loss of hair-cells themselves. To address whether lateral-line overstimulation produced similar morphological changes, we surveyed the number of hair cells per NM and the percentage of NM hair cells lacking afferent innervation in fish immediately following exposure to sustained or periodic stimulation (Fig 3). With periodic exposure, the number of hair cells was comparable to control (Fig 3 D; Unpaired t-test, P=0.9916; n=48-66 NMs; N=4 trials) and there was no significant reduction in afferent innervation of NM hair cells (Fig 3 E; One sample Wilcoxon test, P=0.0625; n=26-39 NMs; N=4 trials). With sustained exposure, we observed a reduction in the number of hair cells per NM immediately following noise (Fig 3 D'; Unpaired t-test, *P=0.0125; n=114-149 NMs; N=13 trials) as well as a significant reduction in the percentage of hair cells per NM innervated by afferent neurons (Fig 3 E'; One sample Wilcoxon test, ****P<0.0001; n=76-103 NMs; N=12 trials).

As described in Fig 2 D, we found on average ~half of the NMs examined showed "disrupted" hair-cell morphology immediately following sustained exposure. To define the associations between overall hair-cell morphology and specific structural changes in noise-

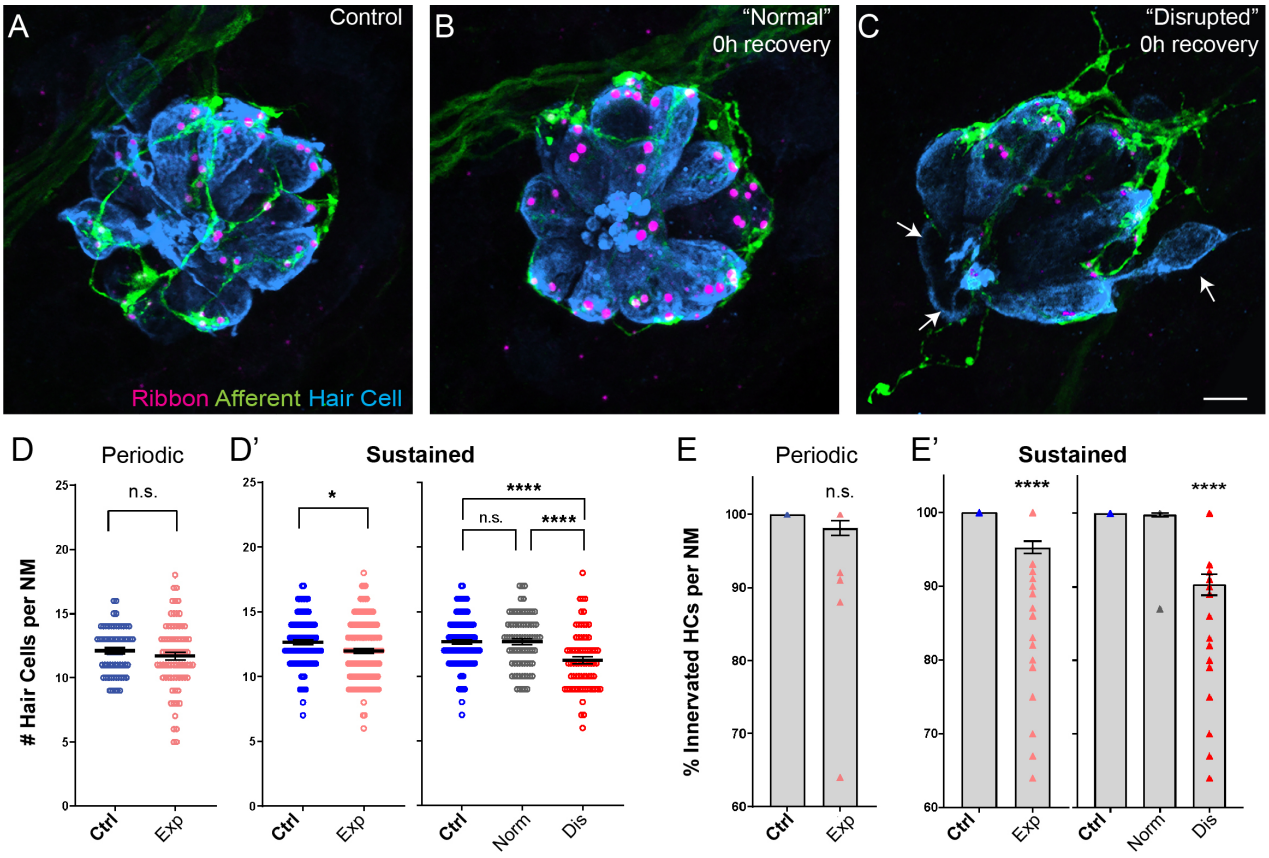

Figure 3: Hair-cell loss and de-innervation is specific to "disrupted" NMs.
(A-C) Representative confocal maximum intensity projection images of control (A), or exposed lateral-line NMs with "normal" (B) or "disrupted" (C) morphology immediately post exposure (0 h). Synaptic ribbons (magenta; Ribeye b) and hair cells (blue; Parvalbumin) were immunolabled. Afferent neurons were labeled with GFP. **(D-D')** Hair-cell number per NM immediately following periodic (D) and sustained (D') exposure. A moderate but significant reduction in hair cell number was observed following sustained exposure (P=0.9916 periodic; *P=0.0125 sustained) and was specific to "disrupted" NMs (D'; P=0.9995 normal, ****P<0.0001 disrupted. Scale bar: 5μm **(E-E')** Percentage of NM hair cells innervated by afferent nerves. A significant percentage of NM hair cells lacked afferent innervation following sustained noise exposure (P=0.0625 periodic; ****P<0.0001 sustained). Hair cells lacking afferent innervation were specifically observed in disrupted NMs (E'; P>0.9999 normal, ****P<0.0001 disrupted).

damaged NMs, we compared the numbers of hair cells per NM and the percent of hair cells innervated in "normal" and "disrupted" NMs. With hair cell number, we observed significant loss specifically in "disrupted" NMs, while "normal" NM hair-cell number appeared comparable to control (Fig 3 D'; Ordinary one-way ANOVA, P=0.9995 (normal), ****P<0.0001 (disrupted)). With hair-cell innervation, we observed a similar trend i.e. a significant number of hair cells lacked innervation in noise-exposed NMs with "disrupted" morphology, but not "normal" NMs (Fig 3 E'; One sample Wilcoxon test, P>0.9999 (normal), ****P<0.0001(disrupted)).

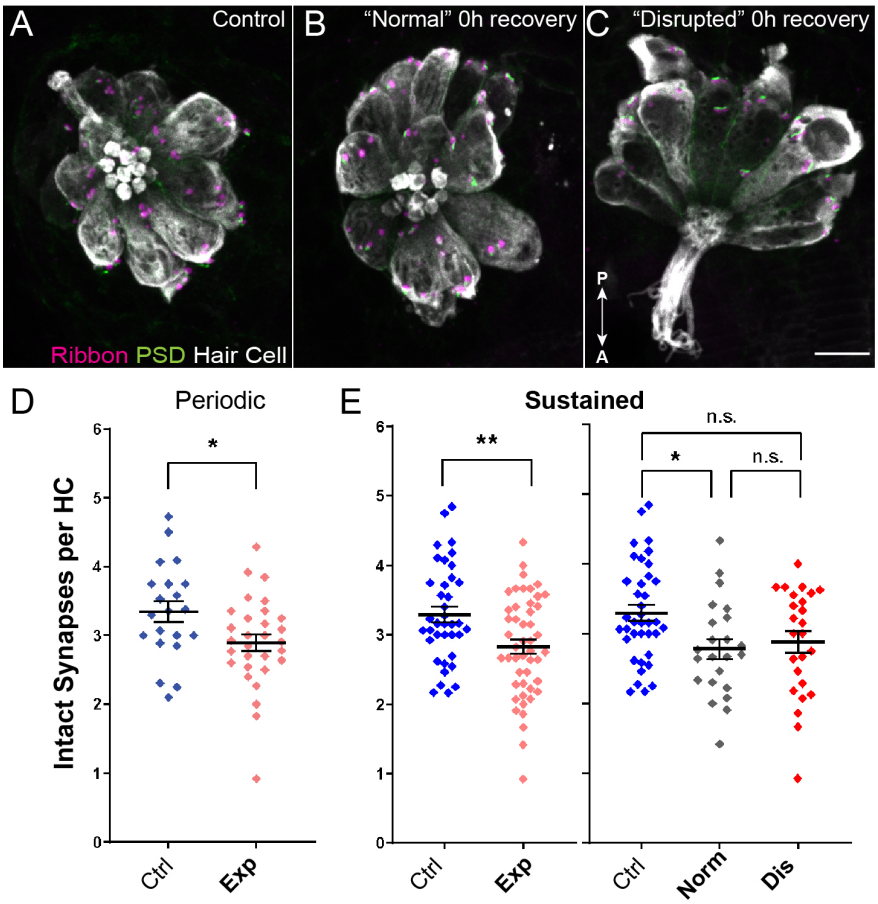

Figure 4: Ribbon synapse loss is more pronounced in "normal" NMs following sustained exposure. **(A-C)** Representative confocal maximum intensity projection images of unexposed (A), or noise exposed lateral-line NMs with "normal" (B) or "disrupted" (C) morphology. Synaptic ribbons (magenta; Ribeye b), PSDs (green; MAGUK) and hair cells (gray; Parvalbumin) were immunolabled. Arrows indicate anterior/posterior axis of orientation. Scale bar: 5μm **(D,E)** The number of intact synapses per hair cell was significantly reduced following either sustained or periodic noise exposure (D; *P=0.0245 periodic, E; **P=0.0036 sustained). (E) Reduced synapse number was more pronounced in "normal" NMs than "disrupted" (*P=0.0213 normal, P=0.0685 disrupted).

We also surveyed the number of afferent synapses in control and overstimulated NM hair cells. Hair cells contain electron-dense presynaptic specializations—called dense bodies or synaptic ribbons—apposing afferent PSDs (Davies, Tingley, Kachar, Wenthold, & Petralia, 2001; Sheets, Trapani, Mo, Obholzer, & Nicolson, 2011). We therefore counted the number of intact synapses (ribbons juxtaposed to PSDs; Fig 4 A-C) in control and exposed larvae. We observed significant reductions in the number of intact synapses per hair cell following both periodic and sustained exposure, with a greater degree of synapse loss in hair cells exposed to sustained stimuli (Fig 4 D,E; Unpaired t-test, *P=0.0245 (periodic), **P=0.0036 (sustained)). When we compared "normal" and "disrupted" NMs following sustained exposure, we observed loss of intact synapses per hair cell in both "normal" and "disrupted" exposed NMs, with significantly fewer synapses in "normal" group relative to control (Fig 4 E; Ordinary one-way ANOVA, *P=0.0213 (normal), P=0.0685 (disrupted)). Taken together, these data revealed that synapse loss was observed in all mechanically overstimulated NM hair cells, including "normal" NMs that showed no loss of afferent innervation.

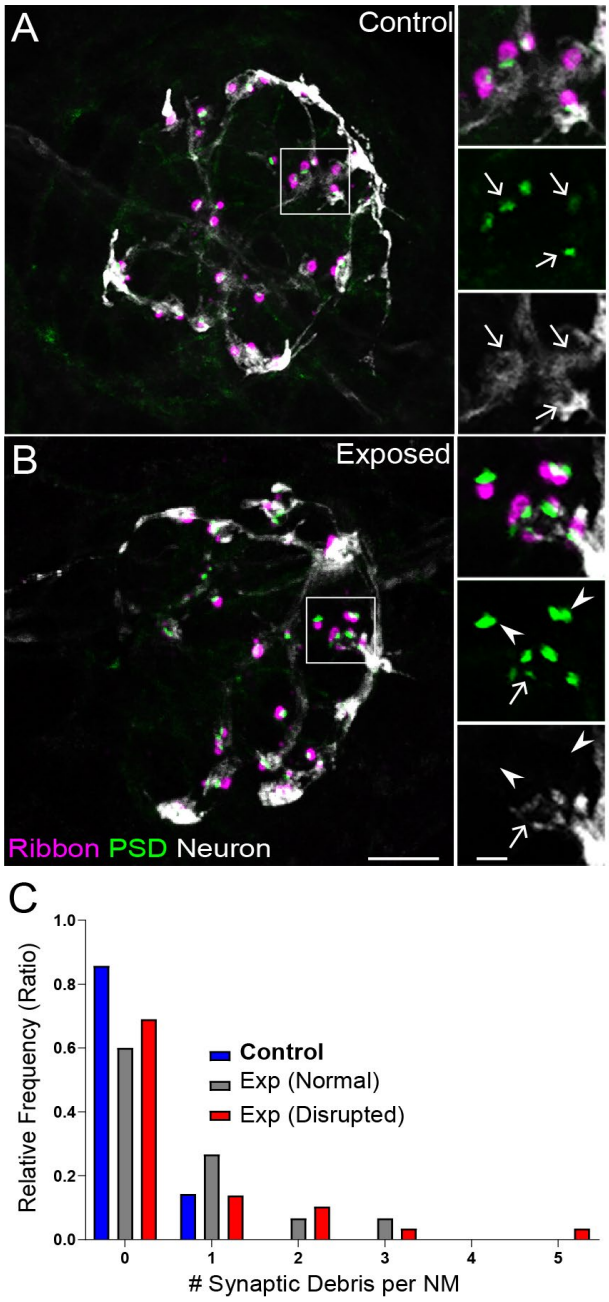

Figure 5: Noise-exposed NMs showed retracted neurites and detached synaptic debris. **(A-B)** Representative images of control (A) and noise-exposed (B) NMs. Synaptic ribbons (magenta; Ribeye b) and PSDs (green; MAGUK) were immunolabeled; hair cells were also immunolabeled, but not shown for clarity. Afferent neurons (white) were labeled with GFP. Insets: Arrows indicate intact synapses adjacent to afferent neurons; arrowheads (B) indicate synaptic debris. Scale bars: 5µm (main panels), 1µm (insets). **(C)** Frequency histogram of observed synaptic debris per NM. While control NMs occasionally had 1 detached synapse, exposed NMs were observed that had up to 5 detached synapses.

These observations also showed that synapse loss in exposed lateral-line hair cells did not match with loss of afferent innervation. To understand why synapse loss did not appear to parallel afferent neurite retraction, we examined fish in which we immunolabeled synaptic ribbons, PSDs, afferent nerve fibers, and hair cells (Fig 5 A,B). We then quantified instances where synapses, i.e. juxtaposed pre- and postsynaptic components associated with hair cells, were no longer adjacent to an afferent nerve terminal. As these synapses appeared detached and suspended from their associated neurons, making them no longer functional, we refer to

them as synaptic debris. While we rarely observed synaptic debris in unexposed NMs, we observed a greater relative frequency of synaptic debris in NMs exposed to sustained stimulus (Fig 5 C; One sample Wilcoxon test, P=0.1250 (control), *P=0.0313(normal), **P=0.0039(disrupted)). These data suggest synapse loss in exposed NM hair cells may be underestimated when quantifying immunolabel of synaptic components alone, since this type of survey does not consider labeled synapses that may no longer be attached to afferent fibers.

Noise-exposed lateral line NMs show signs of hair-cell injury and macrophage recruitment

The inner ears of birds and mammals possess resident populations of macrophages, and additional macrophages are recruited after acoustic trauma or ototoxic injury (Warchol, 2019). A similar macrophage response occurs at lateral line NMs of larval zebrafish after neomycin ototoxicity (Hirose, Rutherford, & Warchol, 2017). Analysis of fixed specimens, as well as time-lapse imaging of living fish, has demonstrated that macrophages migrate into neomycin-injured NMs and actively phagocytose the debris of dying hair cells. To determine whether a similar inflammatory response also occurs after mechanical injury to the lateral line, we characterized macrophage behavior after sustained exposure (as described above, Fig. 2 B). These studies employed Tg(*mpeg1:yfp*) transgenic fish, which express YFP in all macrophages and microglia. Fish were fixed immediately after exposure, or allowed to recover for 2, 4 or 8 hours. Control fish consisted of siblings that received identical treatment, except for the noise exposure. Data were obtained from the two terminal NMs from the pLL of each fish (Fig. 6 A). As also observed in Fig 3 D, a small decline in hair-cell number was apparent in specimens examined immediately after the exposure (Fig. 6 B). Consistent with earlier studies (Hirose et al., 2017), 1-2 macrophages were typically present within a 25 µm radius of each NM (Fig. 6 C). In uninjured (control) fish, those macrophages remained outside the sensory region of the NM and rarely contacted hair cells. However, at 2, 4 and 8 hours after mechanical overstimulation, we observed increased macrophage-hair cell contacts as well as the presence of immunolabeled hair-cell debris within macrophage cytoplasm (suggestive of phagocytosis, Fig. 6 A, E, 4 h., arrow). Notably, the numbers of macrophages within a 25 µm radius of each NM remained unchanged at all time points after noise exposure, suggesting that the inflammatory response was mediated by local macrophages and that mechanical injury did not recruit macrophages from distant locations (Fig. 6 D). This pattern of injury-evoked macrophage behavior is qualitatively similar to the macrophage response observed in the mouse cochlea after acoustic trauma (Hirose et al., 2005; Kaur et al., 2019; Kaur et al., 2015).

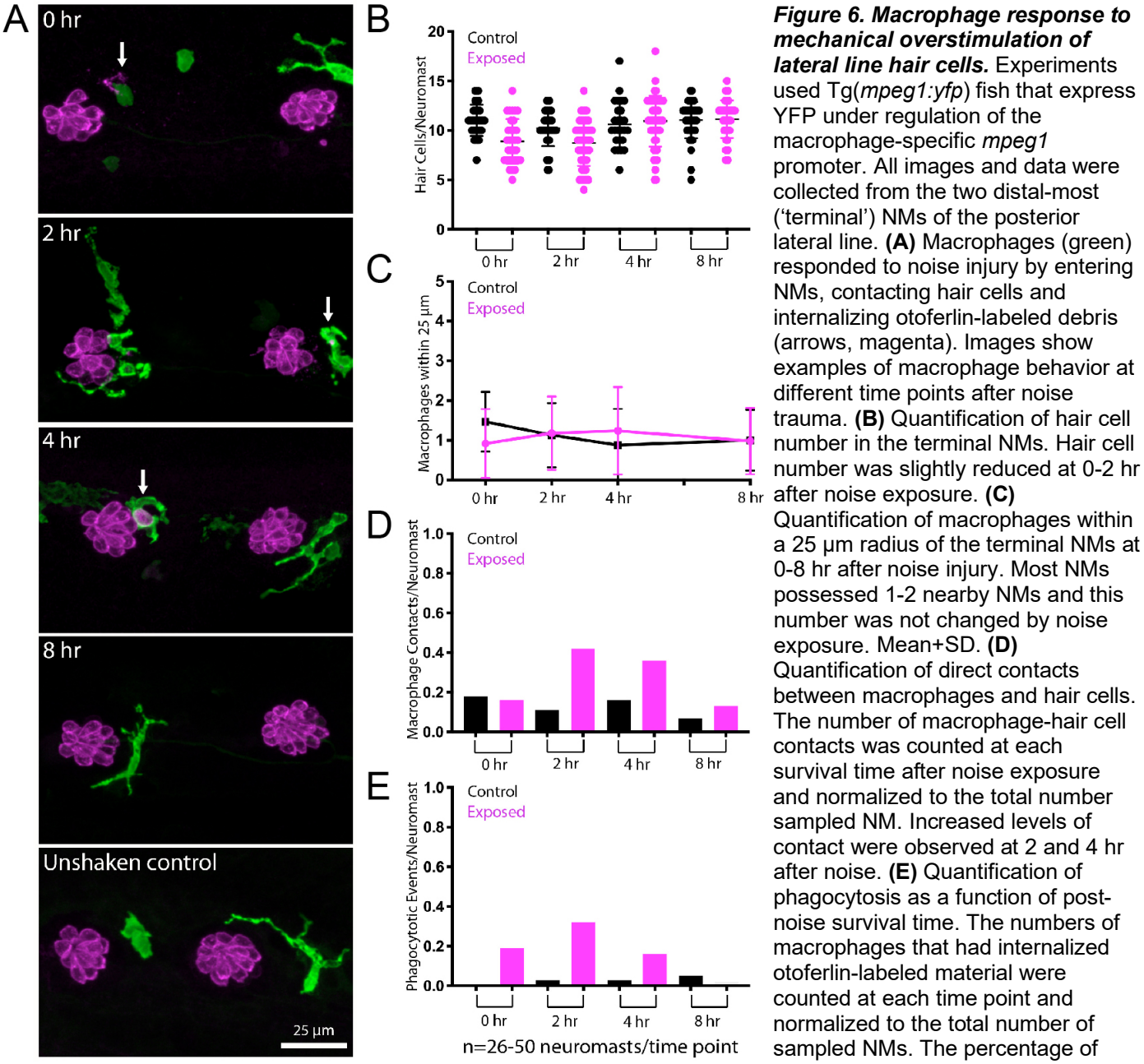

Figure 6. Macrophage response to mechanical overstimulation of lateral line hair cells. Experiments used Tg(*mpeg1:yfp*) fish that express YFP under regulation of the macrophage-specific *mpeg1* promoter. All images and data were collected from the two distal-most ('terminal') NMs of the posterior lateral line. **(A)** Macrophages (green) responded to noise injury by entering NMs, contacting hair cells and internalizing otoferlin-labeled debris (arrows, magenta). Images show examples of macrophage behavior at different time points after noise trauma. **(B)** Quantification of hair cell number in the terminal NMs. Hair cell number was slightly reduced at 0-2 hr after noise exposure. **(C)** Quantification of macrophages within a 25 µm radius of the terminal NMs at 0-8 hr after noise injury. Most NMs possessed 1-2 nearby NMs and this number was not changed by noise exposure. Mean+SD. **(D)** Quantification of direct contacts between macrophages and hair cells. The number of macrophage-hair cell contacts was counted at each survival time after noise exposure and normalized to the total number sampled NM. Increased levels of contact were observed at 2 and 4 hr after noise. **(E)** Quantification of phagocytosis as a function of post-noise survival time. The numbers of macrophages that had internalized otoferlin-labeled material were counted at each time point and normalized to the total number of sampled NMs. The percentage of macrophages that contained such debris was increased at 0-4 hr after noise exposure. Data were obtained from 26-50 NMs/time point.

Overstimulated NMs recover hair-cell shape, hair-cell number, and innervation within hours following exposure

To determine if damage to mechanically overstimulated NMs was progressive, persistent, or reversible, we characterized NM morphology, hair-cell number, innervation, and synapse number at both 2 hours and 48 hours following noise exposure. We observed a decrease in the percentage of NMs showing “disrupted” morphology 2 hours following exposure, relative to fish fixed immediately following exposure (Fig 7 A; 54% disrupted (0 h) vs. 32% disrupted (2 h); N=4 trials), suggesting that disruption of hair-cell morphology following noise is rapidly reversible. Consistent with this observation, the average hair-cell number per NM at 2 hours recovery was similar to control (Fig 7 B; Unpaired t-test, P=0.3011; n=63-75 NMs; N=7 trials). Recovery of hair-cell number appeared to occur within 2-4 hours (Fig 6 A, B) and corresponded with macrophages infiltrating NMs and phagocytosing hair cell debris (Fig. 6 A,E). We also observed, compared to immediately following exposure (Fig 4), a lesser degree of de-innervation (Fig 7 C; One sample Wilcoxon test, ***P=0.0010; n=38-44 NMs; N=6 trials) and synapse loss 2 hours following noise-exposure (Fig 7 D, Unpaired t-test, *P=0.0271; n=37-47 NMs; N=6 trials) indicating some recovery of innervation and synapse number. These observations suggest recovery of hair-cell morphology and replacement of damaged hair cells are concurrent processes in noise-damaged NMs.

A recent study examined zebrafish lateral-line hair cell damage induced by exposure to ultrasonic waves, and reported loss of hair cells 48-72 hours following exposure (Uribe et al., 2018). To determine if lateral line NMs exposed to noise from our apparatus either continued to recover or underwent further delayed damage, we examined hair-cell morphology, number, and innervation 48 hours following noise exposure. Nearly all exposed NMs examined showed “normal” HC morphology (Fig 7 E) with no significant difference in hair-cell number (Fig 7 F; Unpaired t-test, P=0.1253; n=49-57 NMs; N=5 trials). Hair cell innervation after 48 hours was comparable to control fish (Fig 7 G; One sample Wilcoxon test, P>0.9999; n=24-28 NMs; N=5 trials). Synapse number per hair cell also appeared to fully recover (Fig 7 H; Unpaired t-test, =0.7044; n=23-24 NMs; N=5 trials), indicating our overstimulation protocol produces acute and reversible lateral-line damage.

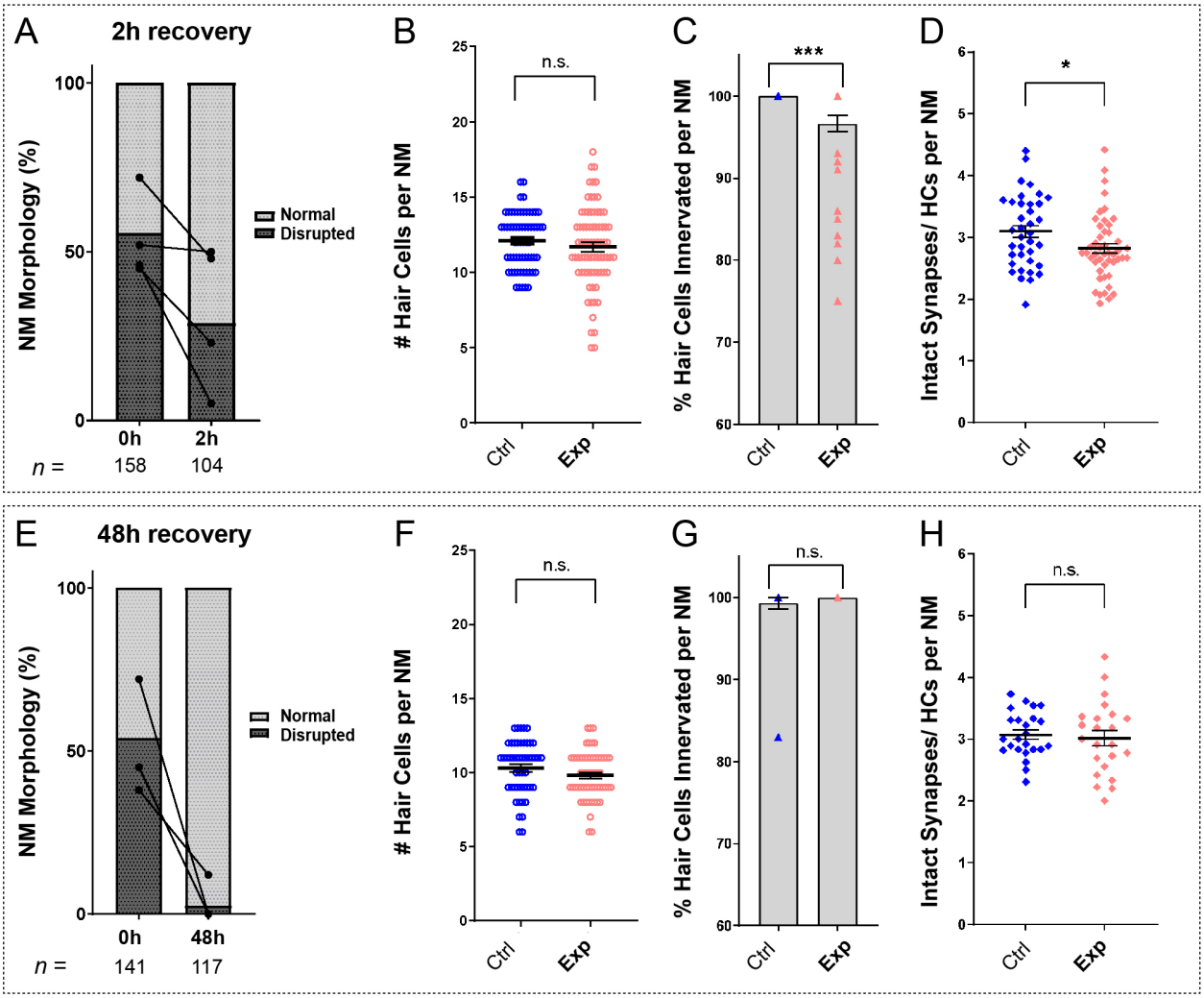

Figure 7: Noise-exposed NMs recover hair-cell morphology, innervation, and synapses by 48 hours following exposure. **(A,E)** Average percentage of exposed NMs with "normal" vs. "disrupted" morphology following exposure. Each dot represents the percentage of disrupted NMs in a single experimental trial; lines connect data points from the same cohort of exposed fish following 2 hours (A) or 48 hours (E) recovery. **(B,F)** Hair-cell number per NM was nearly comparable to control following 2 hour (B, P=0.3011) and 48 hour recovery (F, P=0.1253). **(C,G)** The percentage of NM hair cells lacking afferent innervation was still significant following 2 hour recovery (C, ***P=0.0010), but was fully recovered by 48 hours (G, P>0.9999). **(D,H)** Significantly fewer synapses per hair cell was observed 2 hours following exposure (D, *P=0.0271), but appeared to recover by 48 hours (H, P=0.7044).

PSDs are enlarged in all NMs following noise-exposure

Previous studies in mice and guinea pigs indicate moderate noise exposures modulate the size of synaptic components (Kim et al., 2019; Song et al., 2016). To determine if pre- and postsynaptic components were also affected in our model, we compared the relative volumes of NM hair-cell presynaptic ribbons and their corresponding PSDs in control and noise-exposed larvae. We observed a moderate reduction in synaptic-ribbon size following noise exposure; ribbon volumes were significantly reduced relative to controls following 2 hours recovery (Fig 8

B; Kruskal-Wallis test *P=0.0195; N=3 trials), and this reduction was specific to “disrupted” NMs (Fig 8 C).

While the changes in ribbon volume we observed were modest and delayed in onset, we saw dramatic enlargement of PSDs immediately and 2 hours following exposure (Fig 8 D; Kruskal-Wallis test ****P<0.0001; N=3 trials). In contrast to the observed reduction in ribbon size, relative PSD volumes were significantly enlarged in all noise exposed NMs regardless of whether NM morphology was “normal” or “disrupted” (Fig 8 E). These data reveal enlarged postsynaptic densities as the predominant structural change in noise-exposed NM hair-cell synapses.

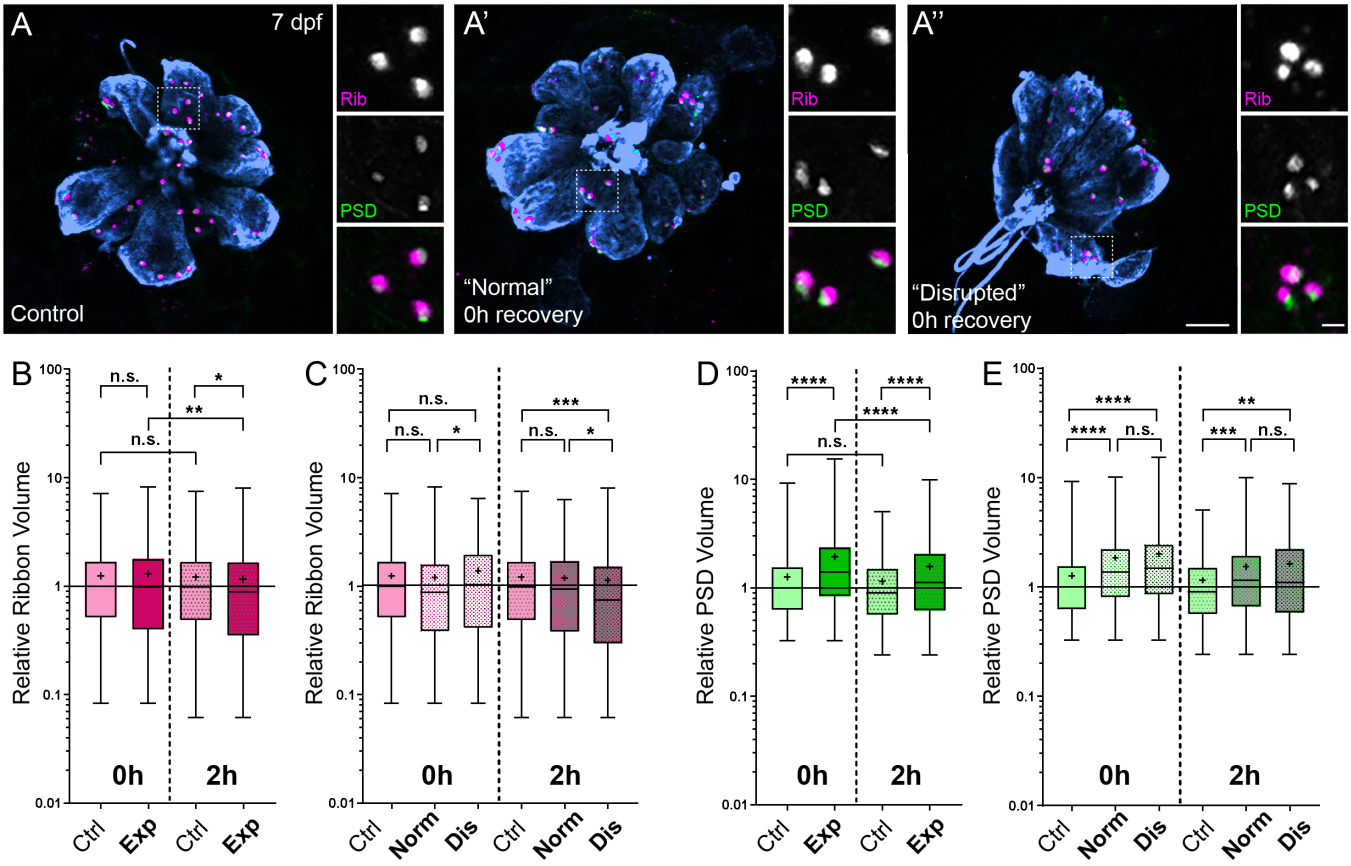

Figure 8: Changes in synaptic ribbon and PSD sizes following noise exposure. **(A-A’’)** Representative images of control (A) and exposed (A’, A”) NMs. Synaptic ribbons (magenta; Ribeye b), PSDs (green; MAGUK), and hair cells (blue, Parvalbumin) were immunolabeled. Scale bars: 5µm (main panels), 1µm (insets). **(B-E)** Box and whisker plots of relative volumes normalized to 0h control. Whiskers indicate the min. and max. values; “+” indicates the mean value. (B) Ribbon volume appeared comparable to control immediately following exposure but was reduced 2 hours after exposure (*P=0.0195). (C) Significant reduction in ribbon size relative to control was specific to disrupted NMs (Kruskal-Wallis test: *P=0.0260 (0h); *P=0.0285, ***P=0.0004 (2h)). (D) Significantly larger PSDs were observed both immediately and 2 hours following noise exposure (****P<0.0001). (E) Enlarged PSDs were present in both “normal” and “disrupted” exposed NMs, with a greater enlargement observed 0h post-exposure (Kruskal-Wallis test: ****P<0.0001 (0h) ; ***P=0.0001, **P=0.0024 (2h)).

Noise-exposed NMs have damaged kinocilia, disrupted hair-bundle morphologies, and reduced FM1-43 uptake

An additional consequence of excess noise exposure is damage to mechanosensitive hair bundles at the apical end of hair cells and, correspondingly, disruption of mechanotransduction (Wagner & Shin, 2019). Larval zebrafish lateral-line hair cells each have a hair bundle consisting of a single kinocilium flanked by multiple rows of actin-rich stereocilia (Kindt, Finch, & Nicolson, 2012). To determine if our exposure protocol damaged apical hair-cell structures, we used scanning electron microscopy (SEM) to assess kinocilia and hair bundle morphology in both unexposed control larvae and larvae fixed immediately following the sustained exposure protocol. All NMs throughout the fish were evaluated, but to remain consistent with our fluorescence imaging results, we closely assessed the appearance of the caudal pLL NMs. We found the caudal NMs to be more damaged than the ones positioned more rostrally: the frequency of NMs with apparently disrupted appearance increased the closer its position to the tail (Fig. 9). This is consistent with our fluorescence observation (Fig. 2 E) in which L5 NMs were more likely to be disrupted than more anteriorly positioned L3. In some extreme cases, terminal NMs appeared engulfed by the surrounding skin, with only the bundle of kinocilia visible through the sleeve-like opening of the skin (Fig. 9 F,G).

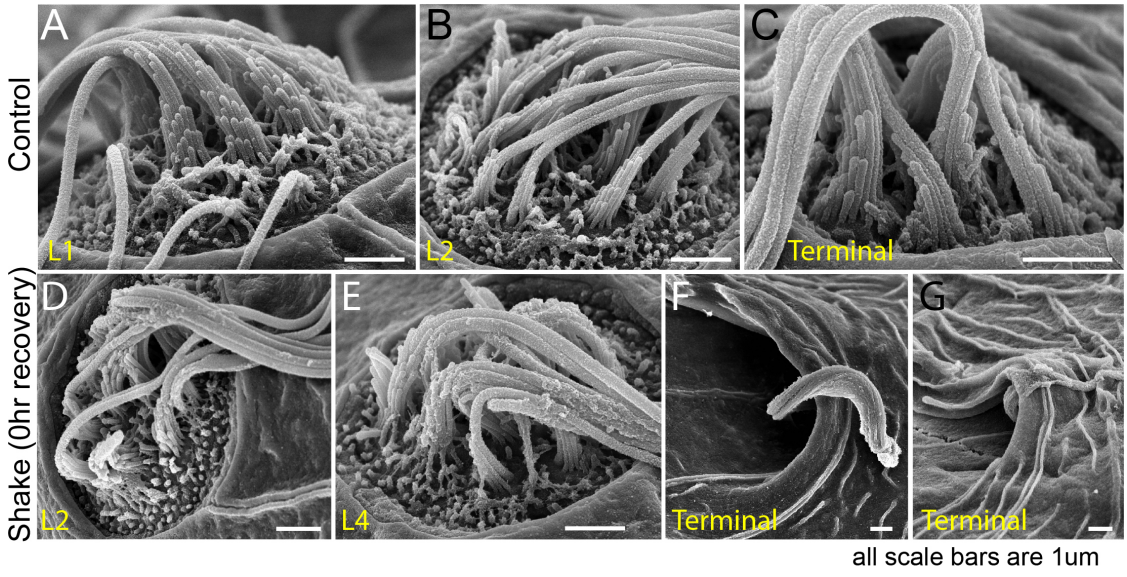

Figure 9: Scanning electron microscopy imaging of tail neuromasts following noise stimulation confirms the damage is more prominent for posterior NMs. **(A-C)** Representative images of tail NMs of control fish larvae, presented as they are positioned on the larva: L1, L2 and terminal NMs. Each hair cell carries a tubulin-based primary cilium (kinocilium), which is thicker than the multiple actin-filled, mechanosensitive stereocilia arranged in a staircase. **(D-G)** Examples of tail NMs immediately following noise exposure, presented as they are positioned on the larva: L2, L4, and two terminal NMs highlighting different levels of damage, with much more pronounced damage evident on terminal NMs. Scale bars: 1 µm.

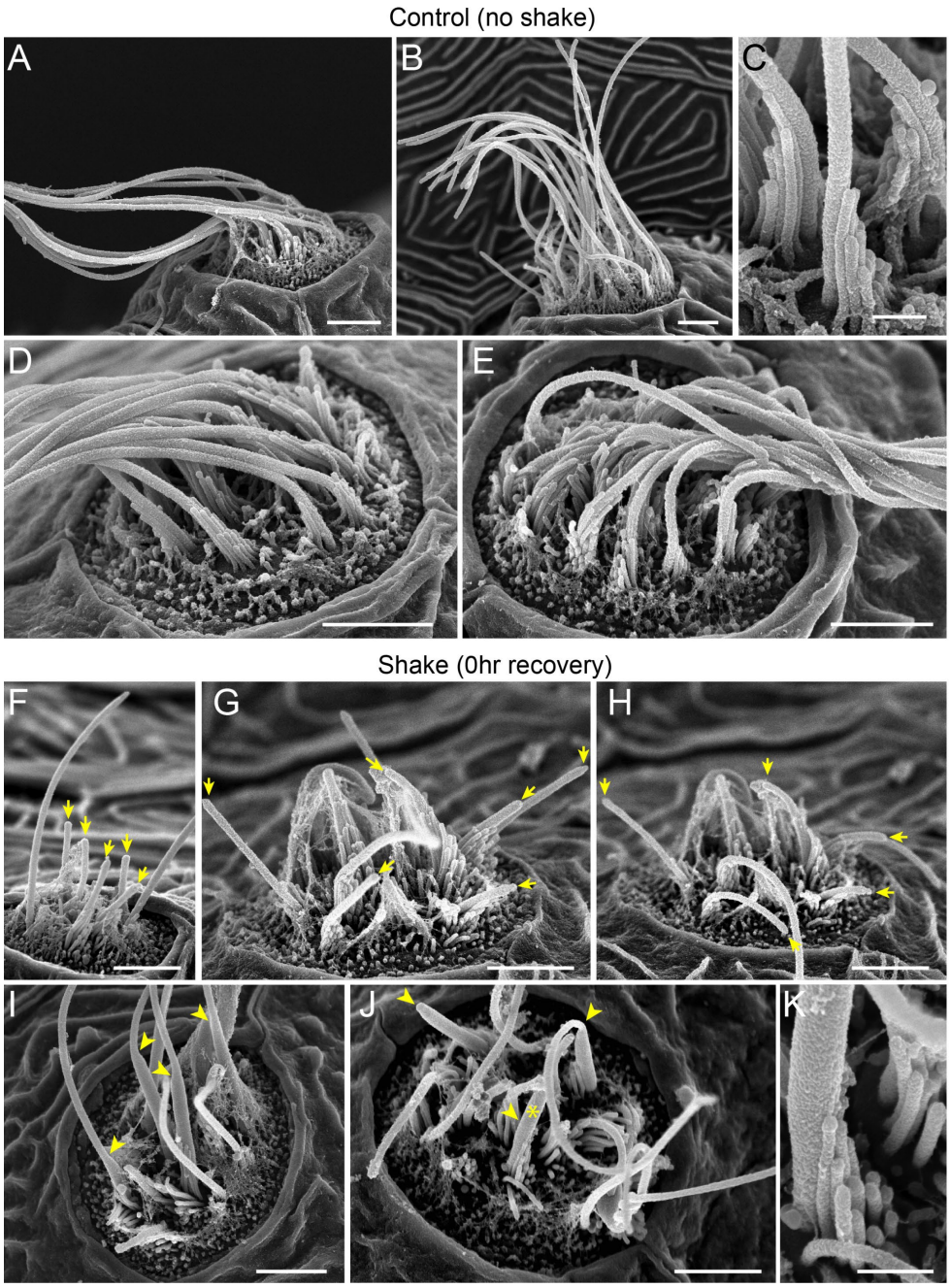

Figure 10: Scanning electron microscopy imaging of neuromasts following noise stimulation reveals disorganized hair cell stereocilia bundles and damaged kinocilia. **(A-E)** Representative images of tail NMs of control fish larvae. Each hair cell carries a kinocilium, which is visibly thicker than its neighboring actin-filled, mechanosensitive stereocilia: see panel C featuring both structures at higher magnification (the kinocilium diameter is 220 nm, while stereocilia measured 90-110 nm). The kinocilia of control NMs are long (10-15 µm) and bundled together, while the stereocilia bundles have an apparent staircase arrangement. **(F-K)** Representative images of damaged tail NMs immediately following noise exposure featuring short (F-H, yellow arrows), disorganized (G, H), and swollen (I-K, yellow arrowheads) kinocilia, and disorganized stereocilia. (K) Same stereocilia bundle as in J marked with an asterisk at higher magnification to highlight the difference in the diameter of the kinocilium (360 nm) and neighboring stereocilia (85-100 nm) for noise exposed hair cells, as compared to the control hair cells in C. Scale bars: A, B, D-J – 2 µm; C, K – 500 nm.

A closer examination of NM morphology revealed a dramatic difference of the kinocilia length and bundling. The NMs of the control fish carry a bundle of long (10-15 µm), uniformly shaped kinocilia (Fig. 10 A-E). In contrast, the NMs of the fish fixed immediately after sustained exposure often appear to carry much shorter kinocilia (Fig. 10 F-H, yellow arrows), which lack bundling and in some cases pointing to different directions (Fig. 10 G,H). The apparent kinocilia length difference between control and overstimulated NMs suggests at least some kinocilia could be undergoing a catastrophic damage event at the time of stimulation, as their distal parts break off the hair cells. This is further supported by some examples of kinocilia with thicker, 'swollen' proximal shafts closer to the cuticular plate of the cell, some of which extend into a thinner distal part while others appear to lack the distal part completely (Fig. 10 I-K, yellow arrowheads). Stereocilia bundles from both groups of animals carried tip links, but we were unable to systematically evaluate and quantify their abundance. However, we observed signs of damaged bundle morphology following overstimulation, as they often appeared splayed, with gaps between the rows of stereocilia.

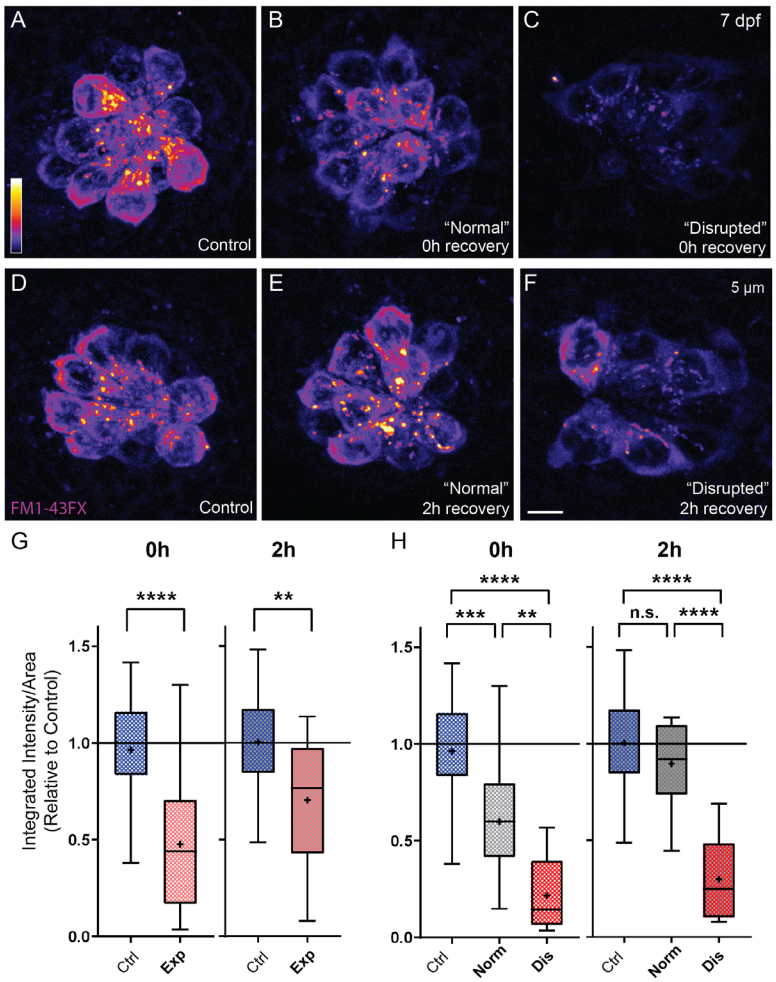

Figure 11: Hair-cell mechanotransduction is reduced following noise exposure. **(A-F)** Representative images of FM1-43FX fluorescent intensity immediately (A-C) or 2 hours (D-F) following noise exposure. Note that fluorescent intensity appears visibly and dramatically reduced in "disrupted" NMs (C,F) and somewhat reduced in "normal" NMs 0h post exposure (B). **(G)** Quantified FM1-43FX fluorescent intensity measurements indicate recovery of mechanotransduction in exposed NMs (Unpaired t-test: ****P<0.0001 (0h), **P=0.0043 (2h)). **(H)** FM1-43FX fluorescence in "normal" exposed NMs is significantly reduced at 0h but appears to fully recover by 2h post-exposure. By contrast, fluorescence intensity in "disrupted" NMs modestly recovered 2h post-exposure. (Ordinary one-way ANOVA ****P<0.0001, ***P=0.0009, **P=0.0078 (0h) ; ****P<0.0001

To determine the effect of noise exposure on hair-bundle function, we assessed mechanotransduction by briefly exposing larvae to the mechanotransduction-channel permeable dye FM1-43 (Toro et al., 2015). While most hair cells showed a dye uptake in both experimental groups, we observed a significant reduction in the relative intensity of FM1-43 immediately following exposure (Fig 11 A-C, G). Reduction of FM1-43 uptake appeared to correspond with the degree of damage to NM hair cells, as we observed notably less relative fluorescence in “disrupted” NMs compared to NMs with “normal” morphology (Fig 11 H). Corresponding to what we observed with hair-cell morphology and number (Fig. 7 A,B), mechanotransduction appears to rapidly recover; 2 hours post noise-exposure FM1-43 uptake is less reduced (Fig 11 D-G) and nearly fully recovered in noise-exposed NMs with “normal” morphology (Fig 11 H). We further observed that FM1-43 uptake after 48 h recovery was comparable to that observed in undamaged (control) fish (Supplemental Figure 2) supporting that hair-cell morphology and function fully recover.

Discussion

To model hair-cell damage resulting from noise in the zebrafish lateral line, we describe here a method to mechanically overstimulate pLL NMs. Using this method we observed i) hair-cell synapse loss and enlarged postsynaptic densities in all exposed NMs, ii) morphological displacement, hair-cell loss, and afferent neurite retraction in a subset of exposed NMs that appeared to correspond with more severe damage, iii) an inflammatory response that peaked 2-4 hours following exposure, iv) kinocilia and hair bundle damage, and v) reduced FM1-43 uptake, indicating damage to mechanotransduction machinery. Remarkably, overstimulated NMs rapidly recover following exposure; NM morphology, innervation, synapse number, and mechanotransduction showed partial recovery within hours and were completely recovered by 2 days post exposure.

Disrupted hair-cell morphology corresponds with more severe mechanical damage

Mechanical overstimulation produced a percentage of pLL NMs that were morphologically “disrupted”. Several observations support that “disrupted” NMs represent more severe injury than overstimulated NMs with “normal” hair-cell morphology. We observed NM disruption more frequently with sustained exposures than with periodic exposures of the same intensity. Moreover, we observed a gradient of disruption, with caudal pLL NMs being more susceptible to mechanically induced disruption than middle pLL NMs. Caudal NMs have been shown to play a more prominent role in detecting water flow velocity and mediating escape bursts than middle or rostral NMs (Olszewski, Haehnel, Taguchi, & Liao, 2012), which may in part explain why caudal NMs are more susceptible to morphological disruption when free-

swimming larvae are exposed to strong current. In addition, “disrupted” NMs showed hair-cell loss and significant afferent neurite retraction, which suggests more severe excitotoxic damage (Sebe et al., 2017). Finally, we observed further reduction of FM1-43 uptake in “disrupted” NMs, suggesting greater mechanical damage to hair bundles (Wagner & Shin, 2019). Our classification of “disrupted” and “normal” NMs is based on their appearance when observed with light microscopy, but a similar trend of “normal” and “disrupted” NMs is evident based on their appearance on SEM (Fig 9). At this time, we are unable to directly correlate the bundle or kinocilia phenotype as seen on SEM of these two classes of NMs to their function as assessed by FM1-43 loading experiments. Our future work will focus on a close evaluation of the FM1-43 uptake and subsequent SEM imaging of the same NM immediately after mechanical overstimulation and following recovery over time.

Hair-cell overstimulation and synapse loss

With both periodic and sustained exposures, we observed hair-cell synapse loss. Two notable observations were made in exposed pLL NMs regarding synapse loss. First, “normal” NMs with no hair cell loss had fewer intact synapses than control (Fig 4 E), suggesting that significant synapse loss occurs even with moderate hair-cell damage. Second, synapse loss occurred in NMs that appeared to be fully innervated (Fig 3 B, Fig 4 B). This observation was more surprising given that pharmacologically blocking postsynaptic Ca^{2+} permeable AMPA receptors (CP-AMPARs), which are evolutionarily conserved and have been shown to drive excitotoxicity and neurite retraction (Sebe et al., 2017), protects against cochlear hair-cell synapse loss from moderate noise exposure (Hu et al., 2020). Additional studies in zebrafish and mice support that mitochondrial calcium influx also contributes to hair-cell synapse loss (Wang et al., 2018; Wong et al., 2019). Future work using this model to examine the effect of noise exposure on mutants with reduced glutamate release or impaired glutamate clearance (to elevate or reduce glutamate in the synaptic cleft, respectively) combined with modified mitochondrial function may define the relative roles of glutamate excitotoxicity and hair-cell mitochondrial stress to synaptic loss.

Role of inflammation following lateral-line overstimulation

Our results indicate that mechanical injury to NMs evokes an inflammatory response. Prior studies of larval zebrafish have shown that macrophages reside near the borders of uninjured NMs and migrate into NMs after ototoxic injury (Hirose et al., 2017). We found that macrophages migrate into NMs within ~2 hours of noise trauma, where they contact hair cells and, in some cases, engulf otoferlin-labeled hair-cell debris. Although this macrophage

response is similar to that which occurs after ototoxic injury to NMs (Carrillo et al., 2016; Hirose et al., 2017), the extent of hair cell loss after noise exposure is much less than the injury that occurs after ototoxicity. We observed macrophage entry in 30-40% of noise exposed NMs, despite minimal hair cell loss (Fig. 6). It is possible that the morphological changes characteristic of “disrupted” NMs are accompanied by the release of macrophage chemoattractants. In addition, studies of noise exposure to the mammalian cochlea indicate that high levels of synaptic activity (without accompanying hair cell loss) can evoke macrophage migration to the synaptic region (Kaur et al., 2019). In either case, the signals responsible for such recruitment remain to be identified. The observation that macrophages had internalized otoferlin-labeled material further suggests that recruited macrophages engage in the phagocytosis of hair cell debris, but it is not clear whether macrophages remove entire hair cells or target specific regions of cellular injury (e.g., synaptic debris; Fig. 5). In any case, our data suggest that the macrophage response to mechanical injury of zebrafish lateral-line neurons is similar to that which occurs after noise injury to the mammalian cochlea (Warchol, 2019) and suggests that zebrafish may be an advantageous model system in which to identify the signals that recruit macrophages to sites of excitotoxic injury.

Hair-cell synapse morphology following mechanical overstimulation

Immediately following mechanical overstimulation, the most pronounced morphological change we observed in hair-cell synapses was significantly enlarged PSDs (Fig. 8 D). Speculatively, PSD enlargement may reflect reduced glutamate release from damaged hair cells. Mice and zebrafish fish lacking hair-cell glutamatergic transmission have enlarged postsynaptic structures (Kim et al., 2019; Sheets, Kindt, & Nicolson, 2012), indicating that glutamate regulates postsynaptic size. While our data do not directly support this idea, we speculate reduced glutamatergic transmission in overstimulated NMs is a likely consequence of damaged hair bundles and impaired mechanotransduction (Zhang et al., 2018). Interestingly, presynaptic ribbons were not similarly enlarged, but instead showed a modest reduction in size following exposure. Functional imaging of zebrafish lateral line has shown that a subset of hair cells in each NM are synaptically silent, and these silent hair cells can become active following damage (Zhang et al., 2018). As ribbon size has been observed to correspond with synaptic activity (Merchan-Perez & Liberman, 1996; Sheets et al., 2012), reduction in ribbon size may reflect recruitment of synaptically silent hair cells following mechanically-induced damage. Future functional studies are needed to determine if mechanical overstimulation recruits more active hair-cell synapses, and to verify whether glutamate release from active synapses is reduced immediately following overstimulation.

Lateral-line NMs completely repair following mechanical damage

Previous studies indicate mammalian cochlear hair cells have some capacity for repair following sub-lethal mechanical damage, including tip-link repair and regeneration of a subset of ribbons synapses (Indzhykulian et al., 2013; Jia, Yang, Guo, & He, 2009; Kim et al., 2019). But such ability is limited, and our understanding of hair-cell repair mechanisms is incomplete. In addition to stereocilia damage, we also found that mechanical trauma resulted in a small degree of hair cell loss (~1-2 hair cell/NM – Fig. 3D'), but that hair cell numbers had recovered after 2 h. (Fig. 7). The mechanism that mediates this recovery is not clear. Hair-cell regeneration in the inner ear can occur via direct phenotypic conversion of a supporting cell into a replacement hair cell (e.g., Warchol, 2011), and it is conceivable that such transdifferentiation could occur within 2 hours of injury. However, the short recovery time is not consistent with the longer process of renewed proliferation and hair-cell differentiation that underlies most hair-cell regeneration in zebrafish and birds (Harris et al., 2003; Ma, Rubel, & Raible, 2008; Romero-Carvajal et al., 2015).

In summary, our data show that mechanical overstimulation of zebrafish lateral-line NMs results in morphological changes in hair cells and loss of afferent synapses, but that these injuries recover within 48 hr. Our next steps will be to define the time course for morphological and functional recovery, and to determine how lateral-line mediated behavior is affected by mechanically induced damage. Sub-lethal overstimulation in the zebrafish lateral line provides a useful model for defining mechanisms of damage and inflammation and for identifying pathways that promote hair-cell repair following sub-lethal noise exposure.

Declaration of interests:
The authors declare no competing financial or non-financial interests

Acknowledgments: This work was supported by the National Institute on Deafness and Other Communication Disorders R01DC016066 (L.S.), R01DC017166 (A.A.I), and R01DC006283 (M.E.W.), Washington University Dept. of Otolaryngology (L.S.), and the Amelia Peabody Charitable Fund (L.S.). We would like to thank Valentin Militchin (WashU) and Evan Foss (Mass Eye and Ear) for engineering support and Mark Rutherford for thoughtful feedback on the manuscript.

Method Details

Ethics Statement

This study was performed with the approval of the Institutional Animal Care and Use Committee of Washington University School of Medicine in St. Louis and in accordance with NIH guidelines for use of zebrafish.

Zebrafish

All zebrafish experiments and procedures were performed in accordance with the Washington University Institutional Animal Use and Care Committee. Adult zebrafish were raised under standard conditions at 27-29°C in the Washington University Zebrafish Facility. Embryos were raised in incubators at 29°C in E3 media (5 mM NaCl, 0.17 mM KCl, 0.33 mM $CaCl_2$, 0.33 mM $MgCl_{2;}$ (Nüsslein-Volhard & Dahm, 2002)) with a 14 h:10 h light:dark cycle. After 4 dpf, larvae were raised in 100-200 ml E3 media in 250-ml plastic beakers and fed rotifers daily. Sex of the animal was not considered in our studies because sex cannot be predicted or determined in larval zebrafish.

The transgenic lines *TgBAC(neurod1:EGFP)* (Obholzer et al., 2008) and *Tg(mpeg1:YFP)* (Roca & Ramakrishnan, 2013) were used in this study. Fluorescent larvae were identified at 2-5 dpf under anesthesia with 0.01% tricaine in E3 media. The *TgBAC(neurod1:EGFP)* line was crossed into casper ($mitfa^{w2/w2}$, $mpv17^{a9/a9}$; (White et al., 2008)). Homozygous carriers $mpv17^{a9/a9}$ were identified at 4-5 dpf by phenotype under a brightfield dissecting microscope based on the severe reduction of iridophores in the eyes (D'Agati et al., 2017).

Experimental Apparatus

Multi-well plates containing larvae were clamped to a custom magnesium head expander (Vibration & Shock Technologies, Woburn, MA) on a vertically-oriented Brüel+Kjær LDS Vibrator, V408 (Brüel and Kjær, Naerum, Denmark). An additional metal plate was fitted to the bottom of the multi-well dish to fill a small gap between the bottoms of the wells and the head expander to eliminate flexing of the well plate relative to the head expander. Vibrometry of the well bottoms and the head expander with a laser-Dopper vibrometer (OFV-2600 and OFV-501, Polytec, Irvine, CA) confirmed that the well plate and head expander motion were equal at stimulus frequencies. This experimental apparatus was housed in a custom sound-attenuation chamber. An Optiplex 3020 Mini Tower (Dell) with a NI PCIe-6321, X Series Multifunction DAQ (National Instruments) running a custom stimulus generation program (modified version of Cochlear Function Test Suite) was used to relay the stimulus signal to a Brüel+Kjær LDS

PA100E Amplifier that drove a controlled 60 Hz vibratory stimulus along the larvae's dorsoventral axis (vertically). Two accelerometers (BU-21771, Knowles, Itasca, IL) were mounted to the head expander to monitor the vertical displacement of the plate. The output of the accelerometers was relayed through a custom accelerometer amplifier (EPL Engineering Core). A block diagram for the EPL Lateral Line Stimulator can be found here: https://www.masseyeandear.org/research/otolaryngology/eaton-peabody-laboratories/engineering-core).

Mechanical overstimulation of lateral-line organs in free swimming larvae

At 7 dpf, free-swimming zebrafish larvae were placed in untreated 6-well plates (Corning, Cat# 3736; well diameter: 34.8 mm; total well volume: 16.8 ml) with 6 ml E3 per well, pre-warmed to 29°C. Up to 15 larvae were placed in each well. Individual wells were sealed with Glad® Press 'n Seal plastic food wrap prior to placing the lid on the plate. An additional metal plate was fitted to the bottom of the multi-well dish to fill a small gap between the bottoms of the wells and the head expander.

Noise exposures (stimulus parameters: 60 Hz, 46.2 ± 0.3 m/s^2) were conducted at room temperature (22-24°C) up to 2 hours after dawn. "Sustained" exposure consisted of 20 minutes of stimulation followed by a 10-minute break and 2 hours of uninterrupted stimulation. "Periodic" exposure consisted of a series of short pulses spanning 2 hours total: 2 20-minute exposures each followed by 10 minutes of rest, followed by 30 minutes of stimulation, a 10-minute break, and a final 20 minutes of stimulation. During the entire duration of exposure, unexposed control fish were kept in the same conditions as noise-exposed fish i.e. placed in a multi-well dish and maintained in the same room as the exposure chamber. After exposure, larvae were either immediately fixed for histology, prepared for live imaging, or allowed to recover for up to 2 days in an incubator at 29°C.

Ablation of lateral-line organ with $CuSO_4$

Free-swimming larvae were exposed to freshly made 3 µM $CuSO_4$ solution in E3 for 1 hour, then rinsed and allowed to recover for 2 hours to ensure complete ablation of the lateral-line NMs. NM ablation was confirmed by immunofluorescent labeling of hair cells.

Fast-start escape response behavior assay

Images of larval swimming behavior (1000 frames per second) were acquired with an Edgertronic SC1 high-speed camera (Sanstreak Corp). Image acquisition began 10 seconds following stimulus onset. All subsequent analysis was performed using ImageJ. To track swimming behavior, images were initially stabilized using the Image Stabilizer Plugin. In stabilized images, the position of individual larval heads (located via the pigmented eyes) in

each frame were tracked using the Manual Tracking Plugin. Larvae were tracked over 10 seconds (10,000 frames total) per trial. 'Fast start' responses—defined as a c-bend of the body occurring within 15 ms followed by a counter-bend— were identified manually.

Whole-mount immunohistochemistry

For visualization of zebrafish lateral-line hair cells, neurons, and synapses: 7-9 dpf larvae were briefly sedated on ice, transferred to fixative (4% paraformaldehyde, 1% sucrose, 37.5 µM $CaCl_2$, 0.1 M phosphate buffer) in a flat-bottomed 2 ml Eppedorf tubes, and fixed for 5 hours at 4-8°C. Fixed larvae were permeabilized in ice-cold acetone for 5 minutes, then blocked in phosphate-buffered saline (PBS) with 2% goat serum, 1% bovine serum albumin (BSA), and 1% DMSO for 2-4 hours at room temperature (RT; 22-24 °C). Larvae were incubated with primary antibodies diluted in PBS with 1% BSA and 1% DMSO overnight at 4-8°C, followed by several rinses in PBS/BSA/DMSO and incubation in diluted secondary antibodies conjugated to Pacific Blue (1:400), Alexa Fluor 488 (1:1000), Alexa Fluor 555 (1:1000), Alexa Fluor 647 (1:1000; Invitrogen), or DyLight 549 (1:1000; Thermo-Fisher) for 2 hours at RT. In some experiments, fixed larvae were stained with 2.5 ug/ml 4′,6-diamidino-2-phenylindole (DAPI; Invitrogen) diluted in PBS to label all cell nuclei. Larvae were mounted on glass slides with elvanol (13% w/v polyvinyl alcohol, 33% w/v glycerol, 1% w/v DABCO (1,4 diazobicylo[2,2,2] octane) in 0.2 M Tris, pH 8.5) and #1.5 cover slips.

For visualization of inflammation and macrophage recruitment: 7 dpf larvae were sedated on ice, transferred to 4% paraformaldehyde fixative in PBS, then fixed overnight at 4-8°C. The next day larvae were rinsed in PBS and blocked in PBS with 5% normal horse serum (NHS), 1% DMSO, and 1% Triton x-100 for 2 hours at RT. Larvae were incubated with primary antibodies diluted in PBS with 5% NHS and 1% Triton-x 100 overnight at RT, rinsed several times in PBS, then incubated in diluted secondary antibodies listed above for 2 hours at RT. Larvae were mounted on glass slides with glycerol/PBS (9:1); coverslips were sealed with clear nail polish.

Primary antibodies

The following commercial antibodies were used in this study: GFP (1:500; Aves Labs, Inc; Cat# GFP-1020), Parvalbumin (1:2000; Thermo Fisher; Cat# PA1-933), Parvalbumin (1:2000; Abcam; Cat# ab11427), Parvalbumin (1:500; Sigma-Aldrich; Cat# P3088), MAGUK (K28/86; 1:500; NeuroMab, UC Davis; Cat# 75-029), Otoferlin (1:500; Developmental Studies Hybridoma Bank/ HCS-1). Custom affinity-purified antibody generated against *Danio rerio* Ribeye b (mouse IgG2a; 1:2000; (Sheets et al., 2011)) was also used.

Live hair cell labeling

To selectively label hair cell nuclei, live zebrafish larvae were incubated with DAPI diluted 1:2000 in E3 media for 4 minutes. Larvae were briefly rinsed 3 times in fresh E3 media, then immediately exposed to noise or drug. To label with FM1-43 vital dye (n-(3-triethylammoniumpropyl)-4-(4-(dibutylamino)-styryl) pyridinium dibromide; ThermoFisher)), free-swimming larvae were exposed to FM 1-43 at 3 μM for 20 seconds, then rinsed 3 times in fresh E3 as previously described (Toro et al., 2015). To label with CellROX^{TM} green reagent (C10444; ThermoFisher), larvae were exposed to 5 μM working solution in E3 for 30 minutes in the dark @ 29ºC, then rinsed 2 times in E3 media and maintained in the dark prior to imaging.

Live imaging of FM1-43 did not provide the temporal resolution needed to compare relative uptake immediately and 2 hours following noise exposure. We therefore examined FM1-43 uptake using the fixable analogue. Free-swimming larvae were exposed to FM 1-43FX at 3 μM for 20 seconds, then rinsed 3 times in fresh E3 and immediately fixed (4% paraformaldehyde, 4% sucrose, 150 μM $CaCl_2$, 0.1 M phosphate buffer). Relative labeling of hair cells at 1-3 hours appeared comparable between live FM1-43 and FM 1-43FX. We also verified loss of FM 1-43FX uptake in larvae following brief treatment with 5 mM BAPTA to disrupt tip links (Kindt et al., 2012). FM 1-43 and FM 1-43FX mean signal intensity from maximum projection images was calculated using ImageJ as the integrated pixel intensity divided by the area of the NM region of interest.

Confocal imaging (fixed specimens)

Images of fixed samples were acquired using an LSM 700 laser scanning confocal microscope with a 63x 1.4 NA Plan-Apochromat oil-immersion objective (Carl Zeiss). Confocal stacks were collected with a z step of 0.3 μm over 7-10 μm with pixel size of 100 nm (x-y image size 51 x 51 μm). Acquisition parameters were established using the brightest control specimen such that just a few pixels reached saturation in order to achieve the greatest dynamic range in our experiments. These parameters including gain, laser power, scan speed, dwell time, resolution, and zoom, were kept consistent between comparisons.

Confocal imaging (live)

Live zebrafish larvae were anesthetized with 0.01% tricaine in E3, then mounted lateral-side up on a thin layer of 1.5-2% low-melt agarose in a tissue culture dish with a cover-glass bottom (World Precision Instruments) and covered in E3 media. Z-stack images with a z step of 0.5 μm (FM1-43) or 1 μm (CellROX^{TM}) were acquired via an ORCA-Flash 4.0 V3 camera (Hamamatsu) using a Leica DM6 Fixed Stage microscope with an X-Light V2TP spinning disc

confocal (60 micron pinholes) and a 63x/0.9 N.A. water immersion objective. Z- acquisition parameters w/ X-light spinning disc: 488 laser “20% power”, 150 ms per frame. Image acquisition as controlled by MetaMorph software.

Confocal image processing and analysis

All analysis was performed on blinded images. Digital images were processed using ImageJ software (Schneider, Rasband, & Eliceiri, 2012). In order to quantitatively measure sizes and fluorescent intensities of puncta, raw images containing single immunolabel were subtracted for background using a 20-pixel rolling ball radius and whole NMs were delineated from Parvalbumin-labeled hair cells using the freehand selection and “synchronize windows” tools. Puncta were defined as regions of immunolabel with pixel intensity above a determined threshold: threshold for Ribeye label was calculated using the Isodata algorithm (Ridler, 1978) on maximum-intensity projections, threshold for MAGUK label was calculated as the product of 7 times the average pixel intensity of the whole NM region in a maximum-intensity projection. Particle volume and intensity were measured using the 3D object counter (Bolte & Cordelieres, 2006) using a lower threshold and a minimum size of 10 voxels. To normalize for differences in staining intensity across experimental trials, all volumes were divided by the median control volume in each trial for each individual channel. The number of particles above lower threshold was quantified using the ImageJ Maximum Finder plugin with a noise tolerance of 10 on maximum-intensity projections. Intact synapses were manually counted and defined as adjoining or overlapping maxima of Ribeye and MAGUK labels. The number of synapses per hair cell was approximated by dividing the number of intact synapses within an NM by the number of hair cells in the NM.

Quantitative data on macrophage response to noise exposure were collected from the two caudal-most (‘terminal’) NMs. Confocal image stacks were obtained using a Zeiss LSM700 microscope and visualized using Volocity software. These image stacks were used to derive three metrics from each NM. First, the number of macrophages within 25 µm of a particular NM was determined by inscribing a circle of 25 µm radius, centered on the NM, and counting the number of macrophages that were either fully or partially enclosed by this circle. Next, the number of macrophages contacting a NM was determined by scrolling through the x-y planes of each image stack (1 µm interval between x-y planes, 15 µm total depth) and the counting macrophages that were in direct contact with Otoferlin-labeled hair cells. Finally, the number of macrophages that had internalized Otoferlin-labeled material (hair cell debris) were counted and were assumed to reflect the number of phagocytic events. For each metric, the recorded number reflected the activity of a single macrophage, i.e., a macrophage that made contacts

with multiple hair cells and/or had internalized debris from several hair cells was still classified as a single 'event.'

Subsequent image processing for display within figures was performed using Photoshop and Illustrator software (Adobe).

Scanning electron microscopy

To image hair cell bundles, zebrafish larvae were noise-exposed then anesthetized in 0.12% tricaine in E3 and immediately fixed in 2.5% glutaraldehyde in 0.1 M sodium cacodylate buffer (Electron Microscopy Sciences) supplemented with 2 mM $CaCl_2$. Larvae were shipped overnight in fixative, then most of the fixative (~90-95%) was removed, replaced with distilled water, and samples were stored at 4C. Next, larvae were washed in distilled water (Gibco), dehydrated with an ascending series of ethanol, critical point dried from liquid CO_2 (Tousimis Aurosamdri 815), mounted on adhesive carbon tabs (TedPella), sputter coated with 5 nm of platinum (Leica EM ACE600), and imaged on Hitachi S-4700 scanning electron microscope.

Statistical analysis

All statistical analyses were performed using Prism 8 (Graphpad Software Inc). Where appropriate, datasets were confirmed for normality using the Kolmogorov-Smirnov test. Statistical significance between multiple conditions with normal distributions was determined by one-way ANOVA and appropriate post-hoc tests; statistical significance between multiple conditions with non-normal distributions was determined by a Kruskal-Wallis test and post-hoc tests. Statistical significance between two conditions was determined by an unpaired Student's *t* test or a Mann–Whitney U test, as appropriate. The one-sample Wilcoxon test was used to calculate the difference between observed and default value. Based on the variance and effect sizes reported previously studies, the number of biological replicates were suitable to provide statistical power to avoid both Type I and Type II error (Sebe et al., 2017; Uribe et al., 2018).

References

Alassaf, M., Daykin, E. C., Mathiaparanam, J., & Wolman, M. A. (2019). Pregnancy-associated plasma protein-aa supports hair cell survival by regulating mitochondrial function. *eLife, 8*. doi:10.7554/eLife.47061

Antonenkov, V. D., Isomursu, A., Mennerich, D., Vapola, M. H., Weiher, H., Kietzmann, T., & Hiltunen, J. K. (2015). The Human Mitochondrial DNA Depletion Syndrome Gene MPV17 Encodes a Non-selective Channel That Modulates Membrane Potential. *The Journal of biological chemistry, 290*(22), 13840-13861. doi:10.1074/jbc.M114.608083

Bhandiwad, A. A., Zeddies, D. G., Raible, D. W., Rubel, E. W., & Sisneros, J. A. (2013). Auditory sensitivity of larval zebrafish (Danio rerio) measured using a behavioral prepulse inhibition assay. *The Journal of experimental biology, 216*(Pt 18), 3504-3513. doi:10.1242/jeb.087635

Bolte, S., & Cordelieres, F. P. (2006). A guided tour into subcellular colocalization analysis in light microscopy. *J Microsc, 224*(Pt 3), 213-232. doi:10.1111/j.1365-2818.2006.01706.x

Bottger, E. C., & Schacht, J. (2013). The mitochondrion: a perpetrator of acquired hearing loss. *Hearing research, 303*, 12-19. doi:10.1016/j.heares.2013.01.006

Bullen, A., Anderson, L., Bakay, W., & Forge, A. (2019). Localized disorganization of the cochlear inner hair cell synaptic region after noise exposure. *Biol Open, 8*(1). doi:10.1242/bio.038547

Burgess, H. A., & Granato, M. (2007). Sensorimotor gating in larval zebrafish. *The Journal of neuroscience : the official journal of the Society for Neuroscience, 27*(18), 4984-4994. doi:10.1523/JNEUROSCI.0615-07.2007

Carrillo, S. A., Anguita-Salinas, C., Pena, O. A., Morales, R. A., Munoz-Sanchez, S., Munoz-Montecinos, C., . . . Allende, M. L. (2016). Macrophage Recruitment Contributes to Regeneration of Mechanosensory Hair Cells in the Zebrafish Lateral Line. *J Cell Biochem, 117*(8), 1880-1889. doi:10.1002/jcb.25487

Cho, S. I., Gao, S. S., Xia, A., Wang, R., Salles, F. T., Raphael, P. D., . . . Oghalai, J. S. (2013). Mechanisms of hearing loss after blast injury to the ear. *PloS one, 8*(7), e67618. doi:10.1371/journal.pone.0067618

Coffin, A. B., Kelley, M. W., Manley, G. A., & Popper, A. N. (2004). Evolution of sensory hair cells. In G. A. Manley, R. R. Fay, & A. N. Popper (Eds.), *Evolution of the Auditory System*. New York: Springer-Verlag.

D'Agati, G., Beltre, R., Sessa, A., Burger, A., Zhou, Y., Mosimann, C., & White, R. M. (2017). A defect in the mitochondrial protein Mpv17 underlies the transparent casper zebrafish. *Developmental biology, 430*(1), 11-17. doi:10.1016/j.ydbio.2017.07.017

Davies, C., Tingley, D., Kachar, B., Wenthold, R. J., & Petralia, R. S. (2001). Distribution of members of the PSD-95 family of MAGUK proteins at the synaptic region of inner and outer hair cells of the guinea pig cochlea. *Synapse, 40*(4), 258-268. doi:10.1002/syn.1048

Fernandez, K. A., Guo, D., Micucci, S., De Gruttola, V., Liberman, M. C., & Kujawa, S. G. (2020). Noise-induced Cochlear Synaptopathy with and Without Sensory Cell Loss. *Neuroscience, 427*, 43-57. doi:10.1016/j.neuroscience.2019.11.051

Gao, W. Y., Ding, D. L., Zheng, X. Y., Ruan, F. M., & Liu, Y. J. (1992). A comparison of changes in the stereocilia between temporary and permanent hearing losses in acoustic trauma. *Hearing research, 62*(1), 27-41. Retrieved from http://www.ncbi.nlm.nih.gov/pubmed/1429249

Glowatzki, E., & Fuchs, P. A. (2002). Transmitter release at the hair cell ribbon synapse. *Nature neuroscience, 5*(2), 147-154. doi:10.1038/nn796

Harris, J. A., Cheng, A. G., Cunningham, L. L., MacDonald, G., Raible, D. W., & Rubel, E. W. (2003). Neomycin-induced hair cell death and rapid regeneration in the lateral line of zebrafish (Danio rerio). *Journal of the Association for Research in Otolaryngology : JARO, 4*(2), 219-234. doi:10.1007/s10162-002-3022-x

Henry, W. R., & Mulroy, M. J. (1995). Afferent synaptic changes in auditory hair cells during noise-induced temporary threshold shift. *Hearing research, 84*(1-2), 81-90. Retrieved from http://www.ncbi.nlm.nih.gov/pubmed/7642458

Hickman, T. T., Smalt, C., Bobrow, J., Quatieri, T., & Liberman, M. C. (2018). Blast-induced cochlear synaptopathy in chinchillas. *Scientific reports, 8*(1), 10740. doi:10.1038/s41598-018-28924-7

Hirose, K., Discolo, C. M., Keasler, J. R., & Ransohoff, R. (2005). Mononuclear phagocytes migrate into the murine cochlea after acoustic trauma. *The Journal of comparative neurology, 489*(2), 180-194. doi:10.1002/cne.20619

Hirose, K., Rutherford, M. A., & Warchol, M. E. (2017). Two cell populations participate in clearance of damaged hair cells from the sensory epithelia of the inner ear. *Hearing research, 352*, 70-81. doi:10.1016/j.heares.2017.04.006

Hu, N., Rutherford, M. A., & Green, S. H. (2020). Protection of cochlear synapses from noise-induced excitotoxic trauma by blockade of Ca(2+)-permeable AMPA receptors.

Proceedings of the National Academy of Sciences of the United States of America, 117(7), 3828-3838. doi:10.1073/pnas.1914247117

Husbands, J. M., Steinberg, S. A., Kurian, R., & Saunders, J. C. (1999). Tip-link integrity on chick tall hair cell stereocilia following intense sound exposure. *Hearing research, 135*(1-2), 135-145. doi:10.1016/s0378-5955(99)00101-x

Indzhykulian, A. A., Stepanyan, R., Nelina, A., Spinelli, K. J., Ahmed, Z. M., Belyantseva, I. A., . . . Frolenkov, G. I. (2013). Molecular remodeling of tip links underlies mechanosensory regeneration in auditory hair cells. *PLoS Biol, 11*(6), e1001583. doi:10.1371/journal.pbio.1001583

Jia, S., Yang, S., Guo, W., & He, D. Z. (2009). Fate of mammalian cochlear hair cells and stereocilia after loss of the stereocilia. *The Journal of neuroscience : the official journal of the Society for Neuroscience, 29*(48), 15277-15285. doi:10.1523/JNEUROSCI.3231-09.2009

Kaur, T., Clayman, A. C., Nash, A. J., Schrader, A. D., Warchol, M. E., & Ohlemiller, K. K. (2019). Lack of Fractalkine Receptor on Macrophages Impairs Spontaneous Recovery of Ribbon Synapses After Moderate Noise Trauma in C57BL/6 Mice. *Front Neurosci, 13*, 620. doi:10.3389/fnins.2019.00620

Kaur, T., Zamani, D., Tong, L., Rubel, E. W., Ohlemiller, K. K., Hirose, K., & Warchol, M. E. (2015). Fractalkine Signaling Regulates Macrophage Recruitment into the Cochlea and Promotes the Survival of Spiral Ganglion Neurons after Selective Hair Cell Lesion. *The Journal of neuroscience : the official journal of the Society for Neuroscience, 35*(45), 15050-15061. doi:10.1523/JNEUROSCI.2325-15.2015

Kim, K. X., Payne, S., Yang-Hood, A., Li, S. Z., Davis, B., Carlquist, J., . . . Rutherford, M. A. (2019). Vesicular Glutamatergic Transmission in Noise-Induced Loss and Repair of Cochlear Ribbon Synapses. *The Journal of neuroscience : the official journal of the Society for Neuroscience, 39*(23), 4434-4447. doi:10.1523/JNEUROSCI.2228-18.2019

Kindt, K. S., Finch, G., & Nicolson, T. (2012). Kinocilia mediate mechanosensitivity in developing zebrafish hair cells. *Developmental cell, 23*(2), 329-341. doi:10.1016/j.devcel.2012.05.022

Kindt, K. S., & Sheets, L. (2018). Transmission Disrupted: Modeling Auditory Synaptopathy in Zebrafish. *Front Cell Dev Biol, 6*, 114. doi:10.3389/fcell.2018.00114

Kniss, J. S., Jiang, L., & Piotrowski, T. (2016). Insights into sensory hair cell regeneration from the zebrafish lateral line. *Curr Opin Genet Dev, 40*, 32-40. doi:10.1016/j.gde.2016.05.012

Krauss, J., Astrinidis, P., Astrinides, P., Frohnhofer, H. G., Walderich, B., & Nusslein-Volhard, C. (2013). transparent, a gene affecting stripe formation in Zebrafish, encodes the mitochondrial protein Mpv17 that is required for iridophore survival. *Biol Open, 2*(7), 703-710. doi:10.1242/bio.20135132

Kujawa, S. G., & Liberman, M. C. (2009). Adding insult to injury: cochlear nerve degeneration after "temporary" noise-induced hearing loss. *The Journal of neuroscience : the official journal of the Society for Neuroscience, 29*(45), 14077-14085. doi:10.1523/JNEUROSCI.2845-09.2009

LeMasurier, M., & Gillespie, P. G. (2005). Hair-cell mechanotransduction and cochlear amplification. *Neuron, 48*(3), 403-415. doi:10.1016/j.neuron.2005.10.017

Ma, E. Y., Rubel, E. W., & Raible, D. W. (2008). Notch signaling regulates the extent of hair cell regeneration in the zebrafish lateral line. *The Journal of neuroscience : the official journal of the Society for Neuroscience, 28*(9), 2261-2273. doi:10.1523/JNEUROSCI.4372-07.2008

McHenry, M. J., Feitl, K. E., Strother, J. A., & Van Trump, W. J. (2009). Larval zebrafish rapidly sense the water flow of a predator's strike. *Biol Lett, 5*(4), 477-479. doi:10.1098/rsbl.2009.0048

Merchan-Perez, A., & Liberman, M. C. (1996). Ultrastructural differences among afferent synapses on cochlear hair cells: correlations with spontaneous discharge rate. *The Journal of comparative neurology, 371*(2), 208-221. doi:10.1002/(SICI)1096-9861(19960722)371:2<208::AID-CNE2>3.0.CO;2-6

Nair, A., Azatian, G., & McHenry, M. J. (2015). The kinematics of directional control in the fast start of zebrafish larvae. *The Journal of experimental biology, 218*(Pt 24), 3996-4004. doi:10.1242/jeb.126292

Nordmann, A. S., Bohne, B. A., & Harding, G. W. (2000). Histopathological differences between temporary and permanent threshold shift. *Hearing research, 139*(1-2), 13-30. Retrieved from http://www.ncbi.nlm.nih.gov/pubmed/10601709

Nüsslein-Volhard, C., & Dahm, R. (2002). *Zebrafish : a practical approach* (1st ed.). Oxford: Oxford University Press.

Obholzer, N., Wolfson, S., Trapani, J. G., Mo, W., Nechiporuk, A., Busch-Nentwich, E., . . . Nicolson, T. (2008). Vesicular glutamate transporter 3 is required for synaptic transmission in zebrafish hair cells. *The Journal of neuroscience : the official journal of the Society for Neuroscience, 28*(9), 2110-2118. doi:10.1523/JNEUROSCI.5230-07.2008

Olivari, F. A., Hernandez, P. P., & Allende, M. L. (2008). Acute copper exposure induces oxidative stress and cell death in lateral line hair cells of zebrafish larvae. *Brain research, 1244*, 1-12. doi:10.1016/j.brainres.2008.09.050

Olszewski, J., Haehnel, M., Taguchi, M., & Liao, J. C. (2012). Zebrafish larvae exhibit rheotaxis and can escape a continuous suction source using their lateral line. *PloS one, 7*(5), e36661. doi:10.1371/journal.pone.0036661

Puel, J. L., Ruel, J., Gervais d'Aldin, C., & Pujol, R. (1998). Excitotoxicity and repair of cochlear synapses after noise-trauma induced hearing loss. *Neuroreport, 9*(9), 2109-2114. Retrieved from http://www.ncbi.nlm.nih.gov/pubmed/9674603

Qiu, X., & Muller, U. (2018). Mechanically Gated Ion Channels in Mammalian Hair Cells. *Frontiers in cellular neuroscience, 12*, 100. doi:10.3389/fncel.2018.00100

Ridler, T. W. C., S. (1978). Picture Thresholding Using an Iterative Selection Method. *3EEE TRANSACTIONS ON SYSTEMS, MAN, AND CYBERNETICS*(8), 630 - 632. doi:https://doi.org/10.1109/TSMC.1978.4310039

Roca, F. J., & Ramakrishnan, L. (2013). TNF dually mediates resistance and susceptibility to mycobacteria via mitochondrial reactive oxygen species. *Cell, 153*(3), 521-534. doi:10.1016/j.cell.2013.03.022

Romero-Carvajal, A., Navajas Acedo, J., Jiang, L., Kozlovskaja-Gumbriene, A., Alexander, R., Li, H., & Piotrowski, T. (2015). Regeneration of Sensory Hair Cells Requires Localized Interactions between the Notch and Wnt Pathways. *Developmental cell, 34*(3), 267-282. doi:10.1016/j.devcel.2015.05.025

Schneider, C. A., Rasband, W. S., & Eliceiri, K. W. (2012). NIH Image to ImageJ: 25 years of image analysis. *Nat Methods, 9*(7), 671-675. doi:10.1038/nmeth.2089

Sebe, J. Y., Cho, S., Sheets, L., Rutherford, M. A., von Gersdorff, H., & Raible, D. W. (2017). Ca(2+)-Permeable AMPARs Mediate Glutamatergic Transmission and Excitotoxic Damage at the Hair Cell Ribbon Synapse. *The Journal of neuroscience : the official journal of the Society for Neuroscience, 37*(25), 6162-6175. doi:10.1523/JNEUROSCI.3644-16.2017

Sheets, L., Kindt, K. S., & Nicolson, T. (2012). Presynaptic CaV1.3 channels regulate synaptic ribbon size and are required for synaptic maintenance in sensory hair cells. *The Journal of neuroscience : the official journal of the Society for Neuroscience, 32*(48), 17273-17286. doi:10.1523/JNEUROSCI.3005-12.2012

Sheets, L., Trapani, J. G., Mo, W., Obholzer, N., & Nicolson, T. (2011). Ribeye is required for presynaptic Ca(V)1.3a channel localization and afferent innervation of sensory hair cells. *Development, 138*(7), 1309-1319. doi:10.1242/dev.059451

Shi, L., Liu, L., He, T., Guo, X., Yu, Z., Yin, S., & Wang, J. (2013). Ribbon synapse plasticity in the cochleae of Guinea pigs after noise-induced silent damage. *PloS one, 8*(12), e81566. doi:10.1371/journal.pone.0081566

Song, Q., Shen, P., Li, X., Shi, L., Liu, L., Wang, J., . . . Yin, S. (2016). Coding deficits in hidden hearing loss induced by noise: the nature and impacts. *Scientific reports, 6*, 25200. doi:10.1038/srep25200

Toro, C., Trapani, J. G., Pacentine, I., Maeda, R., Sheets, L., Mo, W., & Nicolson, T. (2015). Dopamine Modulates the Activity of Sensory Hair Cells. *The Journal of neuroscience : the official journal of the Society for Neuroscience, 35*(50), 16494-16503. doi:10.1523/JNEUROSCI.1691-15.2015

Uribe, P. M., Villapando, B. K., Lawton, K. J., Fang, Z., Gritsenko, D., Bhandiwad, A., . . . Coffin, A. B. (2018). Larval Zebrafish Lateral Line as a Model for Acoustic Trauma. *eNeuro, 5*(4). doi:10.1523/ENEURO.0206-18.2018

Wagner, E. L., & Shin, J. B. (2019). Mechanisms of Hair Cell Damage and Repair. *Trends in neurosciences, 42*(6), 414-424. doi:10.1016/j.tins.2019.03.006

Wang, X., Zhu, Y., Long, H., Pan, S., Xiong, H., Fang, Q., . . . Sha, S. H. (2018). Mitochondrial Calcium Transporters Mediate Sensitivity to Noise-Induced Losses of Hair Cells and Cochlear Synapses. *Front Mol Neurosci, 11*, 469. doi:10.3389/fnmol.2018.00469

Warchol, M. E. (2019). Interactions between Macrophages and the Sensory Cells of the Inner Ear. *Cold Spring Harb Perspect Med, 9*(6). doi:10.1101/cshperspect.a033555

White, R. M., Sessa, A., Burke, C., Bowman, T., LeBlanc, J., Ceol, C., . . . Zon, L. I. (2008). Transparent adult zebrafish as a tool for in vivo transplantation analysis. *Cell Stem Cell, 2*(2), 183-189. doi:10.1016/j.stem.2007.11.002

Wong, H. C., Zhang, Q., Beirl, A. J., Petralia, R. S., Wang, Y. X., & Kindt, K. (2019). Synaptic mitochondria regulate hair-cell synapse size and function. *eLife, 8*. doi:10.7554/eLife.48914

Wynn, T. A., & Vannella, K. M. (2016). Macrophages in Tissue Repair, Regeneration, and Fibrosis. *Immunity, 44*(3), 450-462. doi:10.1016/j.immuni.2016.02.015

Xiao, Y., Faucherre, A., Pola-Morell, L., Heddleston, J. M., Liu, T. L., Chew, T. L., . . . Lopez-Schier, H. (2015). High-resolution live imaging reveals axon-glia interactions during

peripheral nerve injury and repair in zebrafish. *Dis Model Mech, 8*(6), 553-564. doi:10.1242/dmm.018184

Zhang, Q., Li, S., Wong, H. C., He, X. J., Beirl, A., Petralia, R. S., . . . Kindt, K. S. (2018). Synaptically silent sensory hair cells in zebrafish are recruited after damage. *Nature communications, 9*(1), 1388. doi:10.1038/s41467-018-03806-8

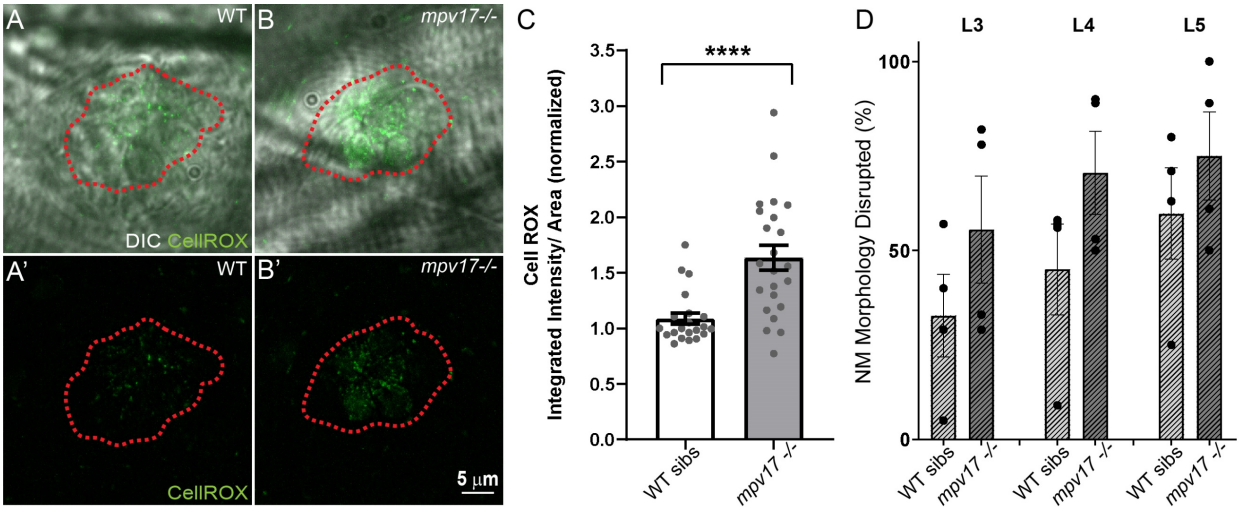

Supplemental Figure 1: mpv17 (-/-) NMs have impaired mitochondrial function and are more vulnerable to noise-induced disruption than WT siblings. **(A-B)** Representative live images of PLL NM3 from an unexposed *mpv17 (-/-)* mutant (B-B') and a WT sibling (A-A'). Red dashed outline indicates the perimeter of the NM hair cells. **(C)** Relative fluorescent intensity measurements of CellROX were significantly higher in unexposed *mpv17 (-/-)* mutant NM hair cells compared to WT (****P<0.0001) **(D)** Average percentage of exposed NMs with "disrupted" morphology following sustained noise exposure. Each dot represents the percentage of disrupted NMs in a single experimental trial. Hair-cell morphology was disrupted more frequently in *mpv17 (-/-)* relative to co-exposed WT siblings.

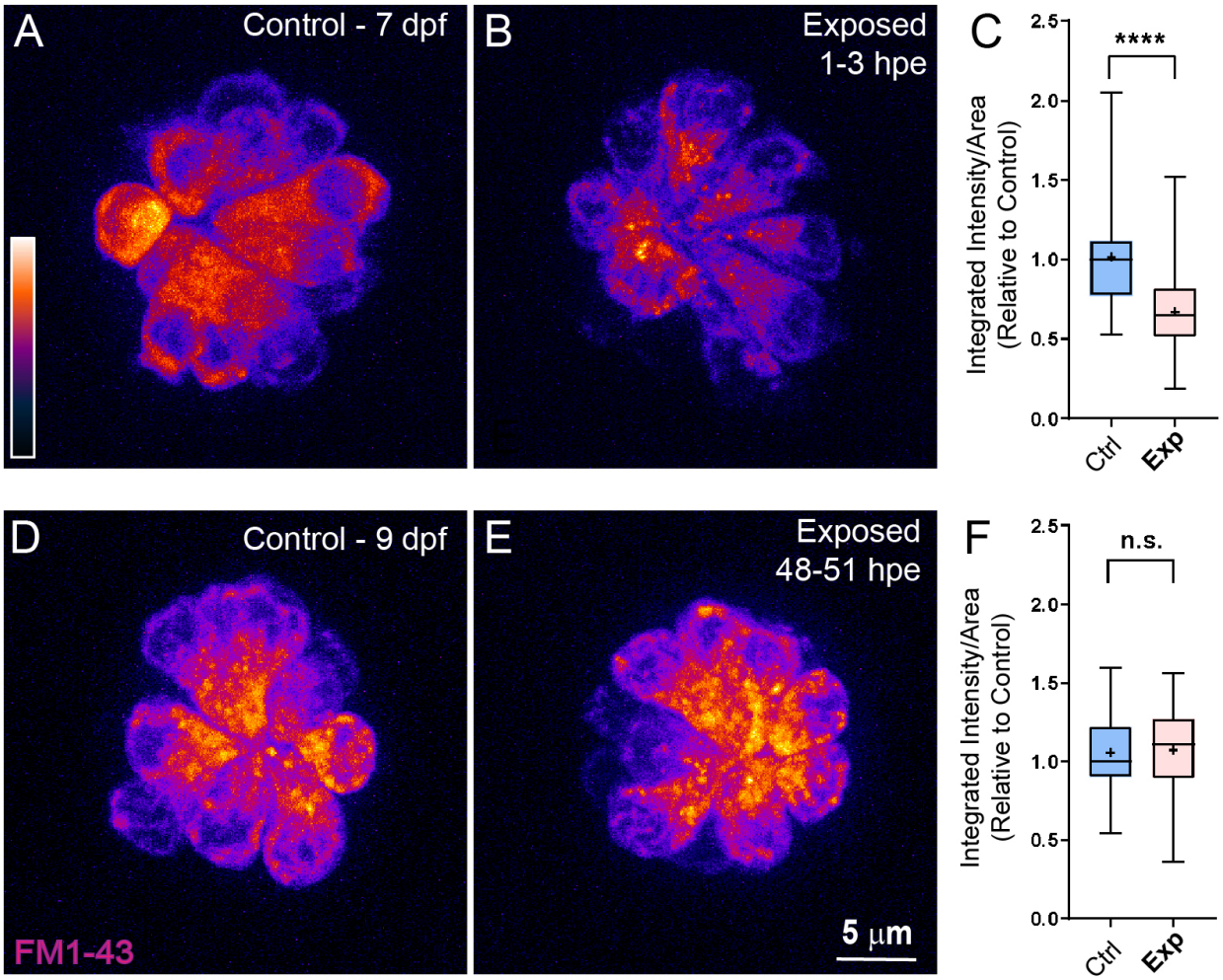

Supplemental Figure 2: Hair-cell mechanotransduction fully recovers following exposure. Representative images of live FM1-43 fluorescent intensity 1-3 hours **(A-C)** or 48-51 hours **(D-F)** following noise exposure. (C) Quantified FM1-43 fluorescent intensity measurements indicate reduced mechanotransduction in exposed NMs (Unpaired t-test: ****P<0.0001). (F) FM1-43 fluorescence fully recovers by 48-51 hours post-exposure.

Supplemental Movies

Swimming behavior of 7-day-old larvae during noise exposure shown in Figure 2 over 500ms (1000 fps/ 500 frames).

Movie S1: Swimming behavior of control fish with intact lateral line organs. Magenta circle indicates a fish prior to a“fast escape” response.

Movie S2: Swimming behavior of larvae whose lateral-line NMs were ablated with $CuSO_4$. Magenta circles indicate larvae that were swept into the waves and could no longer tracked.